UNIVERSITAT POLITÈCNICA DE CATALUNYA

MASTER THESIS

Generalizability of Machine Learning Algorithms for Modelling and Control of Thermostatically Controlled Loads

---

Author:
Attila BÁLINT

Supervisor:
Joaquim RIGOLA
Co-Supervisor:
Hussain KAZMI

September 19, 2018

Abstract

With the proliferation of variable energy sources, flexible energy loads will become more and more important to help stabilize the energy grid. Increasing electrification of heating systems means that the thermal inertia of buildings and hot water vessels can provide a widespread, low cost alternative to electrical storage for providing this energy flexibility.
In this thesis, I demonstrate the modelling capabilities and generalizability of state of the art machine learning techniques on residential hot water systems, using data from multiple large scale real world case studies. I exhibit that an improved control algorithm with these models is capable to reduce the energy consumption of these hot water systems by up to 30%. I also use these models to quantify the effect of major factors influencing available energy flexibility of residential hot water systems. All the houses considered in the analysis feature the same type of hot water system which eliminates any differences in energy flexibility caused by device characteristics. A number of metrics are used from existing literature to quantify flexibility, and find that ambient conditions, control algorithm and occupant behaviour all play significant but very different roles. There are also some key differences in the way these factors influence energy demand and flexibility. The available capacity and recovery periods can differ by as much as two to four times for the same storage vessel, meaning that these differences have to be taken into account during operational planning with flexible loads.
We conclude with a discussion on the implications of hot water system modelling and its generalizability, the variations in flexibility they can provide and the controllers that can be adopted to influence it in practice.

Keywords: hot water systems, residential buildings, modelling, energy flexibility, occupant behaviour, heat pumps, control algorithm

Acknowledgements

I would like to express my deepest gratitude towards my mentor Hussain at Enervalis for his invaluable guidance and support academically and personally throughout my internship. Thanks to him, my knowledge and interest in the data science field has been greatly expanded. I would also like to take this opportunity to be grateful for the generous support from my supervisor Joaquim Rigola at UPC, who has shown great interest in my work and continuously given me advices to improve my thesis. My deepest thanks are also extended to my colleagues Igor, Brecht, Tim, Koen, etc at Enervalis for their company and our fun lunches together.
Last but not least, I would like to thank my friends and my beloved one for their unwavering support and understanding throughout these 2 years.

Contents

List of Figures

List of Tables

List of Abbreviations

ADR	**A**ctiv **D**emand **R**esponse
BP	**B**ack **P**ropagation
DHW	**D**omestic **H**ot **W**ater
EED	**E**nergy **E**fficiency **D**irective
EPC	**E**nergy **P**erformance **C**ertificate
FIT	**F**eed **I**n **T**ariff
HP	**H**eat **P**ump
HVAC	**H**eating **V**entillation and **A**ir **C**onditioning
IEA-EBC	**I**nternational **E**nergy **A**gency's **E**nergy in **B**uildings and **C**ommunities Programme
KPI	**K**ey **P**erformance **I**ndicator
MAE	**M**ean **A**bsolute **E**rror
MLP	**M**ulti**L**ayer **P**erceptron
nZEB	**n**ear **Z**ero **E**nergy **B**uilding
NN	**N**eural **N**etrork
RBC	**R**ule **B**ased **C**ontroller
RES	**R**enewable **E**nergy **S**ources
RL	**R**einforcement **L**earning
TCL	**T**hermostatically **C**ontrolled **L**oad
TES	**T**hermal **E**nergy **S**torage

List of Symbols

E	energy	$\mathrm{W\,h}$ (J)
P	power	W ($\mathrm{J\,s^{-1}}$)
Q	flow	$\mathrm{m^3\,s^{-1}}$ ($\mathrm{L\,h^{-1}}$)
T	temperature	°C
V	volume	$\mathrm{m^3}$ (L)

Chapter 1

Introduction

1.1 From energy efficiency to energy flexibility

The biggest environmental challenge in the 21th century will be the mitigation of climate change. [1]To reduce the risks and impacts of it, more than 170 countries signed the Paris Agreement at COP21, which aims to limit the temperature increase below 2 °C compared to pre-industrial levels [2]. In alignment with these goals, the European Commission introduced a set of *Energy Efficiency Directives* (EED) [3], from which *the 2020 energy & climate package* is currently in force [4]. One of the three key targets of this directive is to increase the energy efficiency by 20 % until 2020, which was later updated to 30 % by 2030 [5]. They all emphasise the buildings and the renovation of the building stock, as commercial and residential buildings in the European Union are responsible for 40 % of final energy consumption and 36 % of CO_2 emissions with a clear potential of energy efficiency increase, since around 75 % of them are inefficient [6]. Beside the EED, the *Energy Performance of Buildings Directive* [7] was especially developed to regulate the sector. Under the existing directive:

- energy performance certificates (EPC) are to be included in all advertisements for the sale or rental of buildings
- EU countries must establish inspection schemes for heating and air conditioning systems or put in place measures with equivalent effect
- all new buildings must be nearly zero energy buildings (nZEB) by 31 December 2020 (public buildings by 31 December 2018)
- EU countries must set minimum energy performance requirements for new buildings, for the major renovation of buildings, and for the replacement or retrofit of building elements (heating and cooling systems, roofs, walls and so on)
- EU countries have to draw up lists of national financial measures to improve the energy efficiency of buildings.

The EPCs are demonstrated to have a positive impact on the housing market by increasing transparency about the costs [8], however they are often criticised as they do not resemble real consumption dynamics. They are calculated based on a steady state energy balance performed at single building level assuming standard boundary conditions and constant building use, therefore they do not take into account the influence of occupant behaviour or real time CO_2 emissions of the consumed energy [9, 10].

One of the proposed solutions to achieve the set targets by the EED is the large-scale integration of renewable energy sources (RES) into the energy systems, which happens in many countries parallel with the increasing electrification of demand e.g. electric cars or electrical heating such as heat pumps. These changes in the supply and demand side create new challenges to the management of the energy systems with greater variability and limited controllability of the RES, require more complex control and shorter decision times [11, 12]. Furthermore, it will desire a change from the traditional energy systems where production follows the demand, to a new flexible one, in which demand is able to respond to production as well. The wholesale electricity markets need to evolve with these changes to allow shorter term trading and also reward flexibility for generation, demand and storage.

With the decentralization of conventional generation, smart and interconnected markets will also make it easier for consumers to generate, store, share, consume or sell back their electricity to the market. Consumers will also be able to offer demand response and actively manage their energy through innovative services [3]. Being major consumers, buildings may significantly contribute to increasing flexibility of the demand in the energy system, as large portion of their energy demand may be shifted in time [13]. In particular, the thermal part of the energy demand, e.g. space heating/cooling, ventilation, domestic hot water, but also hot water for washing machines, dishwashers and heat to tumble dryers can be shifted. However, there is no overview or insight into how much energy flexibility different building types and their usage may be able to offer to the future energy systems. Therefore the International Energy Agency's Energy in Buildings and Communities Programme (IEA-EBC) launched a new research programme, Annex 67, with the following objectives [14]:

- Development of common terminology and definition of Energy Flexibility in buildings and a classification method
- Investigation of user comfort, motivation and acceptance associated with the introduction of Energy Flexibility measures in buildings
- Investigation of the Energy Flexibility potential in different buildings and contexts, and development of design examples, control strategies and algorithms
- Investigation of the aggregated Energy Flexibility of clusters of buildings and the potential effect on energy grids
- Demonstration of Energy Flexibility in buildings through experimental and field studies

This thesis aims to contribute to the research of the Annex 67 by assessing the potential flexibility of thermostatically controlled loads (TCLs), more specifically domestic hot water tanks by using state of the art modelling techniques.

1.2 The scope of the thesis

The conducted research, which this thesis is based on were performed on real world data collected from different European renovation projects. Data is being collected from multiple devices e.g. photovoltaic panels, smart electricity meter, battery and thermal storage units. The vast amount of collected data makes it possible to use state of the art modelling and controlling techniques such as deep neural networks and multi agent reinforcement learning. As model-based reinforcement learning outperforms the model-free counterpart in multiple key areas such as learning time and performance [15], this thesis is focusing on the modelling of domestic hot water tanks using deep neural networks, which can serve as a base of such control algorithm. This work does not investigate the performance of other kinds of machine learning models, as NN showed the highest potential during previous research [16]. Building on the previous research by Kazmi et al., which demonstrated that the multi agent learning framework clearly outperforms the single agent ones [17], this thesis aims to demonstrate the generalisability and reusability of such models.

The learnt models in combination with the raw data allowed the creation of a simulation framework. This framework can be used for various reasons as demonstrated in this thesis:

- Assess the performance of different modelling and control strategies.
- Estimate the potential flexibility of the hot water tank.
- Analyse the effect of occupant behaviour.
- Evaluate the pressure on the grid based on the demand.

1.3 Structure

The thesis structured in the following manner. The following chapter (Chapter 2) introduces the definitions and indicators of energy flexibility, then reviews the related literature on modelling and control of thermostatically controlled loads (TCLs) and contains a brief introduction into the machine learning terminology used in this thesis. Chapter 3 describes the workflow of this thesis, starting with the collected data, followed by data pre-processing and feature engineering and the steps during the model training, validation and prediction. It also describes the used simulation framework and the investigated control mechanisms. The calculated flexibility indicators are also explained in greater detail in this chapter. The obtained results are presented in detail in chapter 4 starting with the results on model performance followed by the results from different control strategies and on flexibility. The insights made from the results can be found in chapter 5 followed by the conclusions of the thesis in chapter 6.

Chapter 2

Background Literature

2.1 Energy flexibility

2.1.1 Definition of energy flexibility

It is difficult to find a common definition of energy flexibility as the different parties involved (households, grid operator, energy supplier etc.) have different objectives when talking about flexibility. Flexibility can be viewed as an *ability* to change from reference scenario, a *property* of an equipment or a building, even as a *service* which can be provided to other parties. After an extensive literature review [18–25], three dimensions appear commonly between the different definitions:

1. Capacity (amount of energy that can be shifted per time unit, including the direction of the shift)
2. Time (like starting time & duration)
3. Cost (potential cost saving or energy use associated to activating the available flexibility)

As a general definition proposed within the Annex, energy flexibility of a building is the ability to manage its demand and generation according to local climate conditions, user needs and grid requirements. Energy flexible buildings will thus allow demand side management/load control and thereby demand response based on the requirements of the surrounding grids and on availability of RES, in order to minimize the CO_2 emissions.

Energy flexibility can be obtained by a high level of controllability, based on the technical constrains of the system and the boundary conditions from the surroundings, while maintaining the occupant comfort. Energy flexibility is activated by an external signal, many times referred to as penalty signal. The penalty signal can be designed to minimize the energy consumption, the costs, the CO2 footprint of the building or a combination of any of those. As there are many low and high frequency influencing factors, which act as boundary conditions, energy flexibility is not a static value, but highly varies over time. High frequency influencing factors are e.g. hourly energy prices, user behaviour, ambient temperature, while some of the low frequency ones are e.g. climate change, energy costs, technological improvement. This makes it required to have a detailed dynamic model of the system in order to accurately assess the flexibility potential [26].

Some form of demand response has been implemented into the power grids for a long time, with forms ranging from load shedding for blackout prevention, to time of use rates to reduce system peak load. Even though advancement in computation and communication

technology would allow more advanced forms of demand response, the lack of harmonised standards and protocols still act as a barrier, while control and market structures for demand response are currently under research [27].

2.1.2 Indicators of energy flexibility

Multiple recent research aim to extend the building energy metrics from performance and energy efficiency to energy flexibility.

When focussing on building energy self-sufficiency, a self-consumption factor, also knows as supply cover factor (γ_s) measures the proportion of energy consumption covered by local generation. A value of 0 represents no local generation consumed in the building, whereas 1 indicates that all local generation was consumed locally. Similar to self-consumption, self-generation or load cover factor (γ_l) defines the proportion of the electricity demand met by on-site generation. A value 0 indicates that no local energy consumption was covered by local generation, while 1 means that all energy consumption was covered by local production [28].

Le Dréau and Heiselberg introduced a flexibility factor (FF) to measure load shifting from high price periods. The FF ranges between -1 and 1 for a given cost reference C_0. If all energy is consumed during low pricing, FF maximises at 1, while if all energy is consumed during the high pricing period, the FF equals to -1 [29].

Reynders et al. measure the flexibility due to the thermal mass of buildings called structural thermal energy storage. C_{ADR} is the available storage capacity, while η_{ADR} is defined as storage efficiency. Both of them varies with time depending on boundary conditions including climate, occupants and heating system and both of them are building characteristics. The power shifting capacity l_{shift} is the difference in heating power during ADR (l_{ADR}), and the reference heating power during l_{ref} normal operation [30].

The review by Stinner et al. categorises operational flexibility as either temporal flexibility, power flexibility or energy flexibility. Energy flexibility is a combination of temporal and power flexibility [31]. They refer to forced and delayed flexibility discussed a few years prior by Nuytten et al. [32]. Delayed flexibility quantifies the number of hours the heat generation can be delayed, while the load still met drawn from the initially fully charged thermal energy storage (TES). On the other hand, forced flexibility is the duration that the heating source can be forced to operate, while storing excess energy, starting with an empty TES.

These proposed key performance indicators (KPIs) vary by control strategy as described in [33]. Different metrics of self-consumption and grid feed-in apply to RPC and cost-optimal control respectively. As expected, self-consumption predominates where feed-in-tariffs (FITs) are lower than the energy price or non-existent.

IEA Annex 67 is aiming to standardise the methodology in which energy flexibility is calculated, in order to increase the comparability between studies. An abstract formulation was proposed whereby the system's response to a step change in the penalty signal defines the energy flexibility potential (Fig. 2.1). As indicated in figure 2.1, Energy Flexibility indicators can be derived in standardised way that characterise the system and that are easily communicated and interpreted between engineers and other stakeholders. In response to these signals, the controller should minimize the penalty, and the capacity of the building to respond to the signal represents the Energy Flexibility. Theoretically,

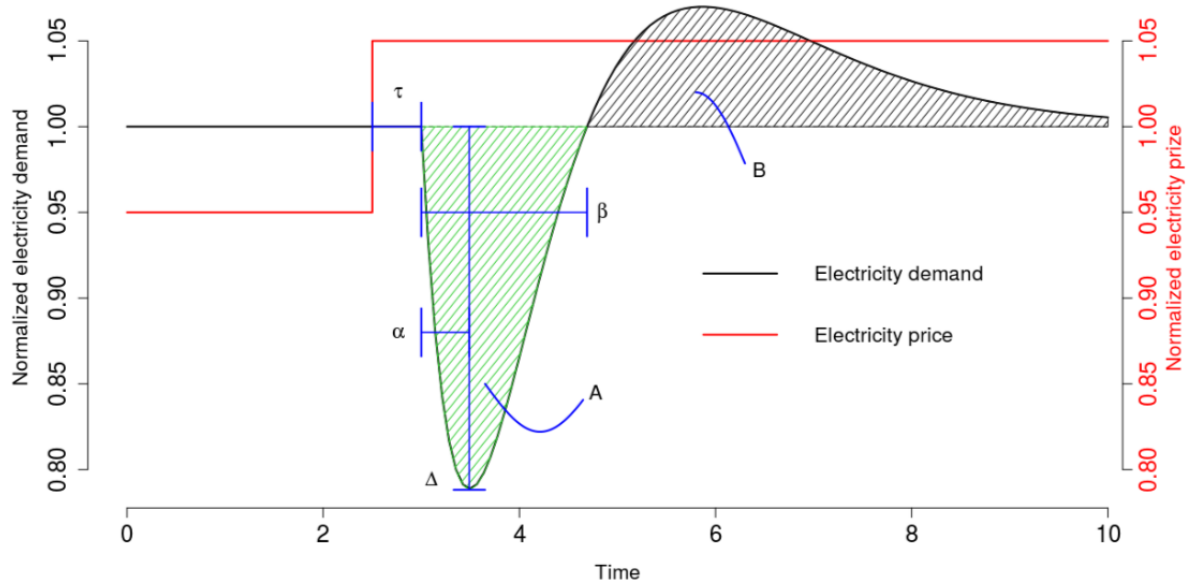

FIGURE 2.1: Response of a building's electricity demand to a penalty signal where τ is the time from the signal is submitted until the start of the action, α is the period from start of the response to the max response, Δ is the maximum response, β is the duration of the response, A is the shifted amount of energy, B is the rebound effect for returning the situation back to "reference" [26]

this method can be applied on various levels in the energy system, going from clusters of buildings down to individual technologies [26].

2.2 Thermal energy storage modelling

Modelling and simulations allow engineers to investigate and analyse physical systems so that design flaws or failures can be avoided before being deployed in practice. Models and simulations can serve different purposes. Here, the discussion is focused on models of buildings and thermal energy storage (TES) systems, created for control purpose, given that these two components contribute directly to the energy flexibility of buildings. Modelling approaches can be generally divided into two parts: modelling of the building itself and modelling of mechanical and thermal systems supplying service to buildings, such as heating, ventilation, and air conditioning (HVAC), domestic hot water (DHW) system, solar thermal collectors, photovoltaics etc. From the degree how detailed a model represents a building, a building model in the literature can be roughly categorized into three groups: white-box, grey-box and black-box models.

The white-box model, also called physical model, describes a building in detail based on building physics. These models are based on the physical properties such as geometry, material properties and thermodynamic laws. White-box models are easily usable and understandable for people familiar with building physics as these parameters are represent real-world properties of the building. Building performance simulation programs commonly used by building modellers all adopt this approach and they are able to model systems in great details, even before it is being built. On the other hand such detailed

models suffer from model complexity due to the large amounts of input parameters [34], which not just makes it expensive to create, but also unfeasible in real-time control applications due to high computational demand. Besides offline control application, the white-box model is more often used to generate a synthetic database which is further utilized for system identification and validation of simplified models.

Black box models, also called data-driven models on the other hand are based on measured input and output data, deriving the connection with mathematical and statistical models, so they can only be used after construction. They often use machine learning algorithms, such as autoregressive moving average (ARMA), artificial neural networks (ANN) and so on [35, 36]. In ANNs the model parameters are the number of neurons and the values of interconnection weights, which do not have any physical meaning, thus they are much harder to interpret than white-box models. The modelling time on black-box models is highly dependent on the available tools and the expertise of the modeller, but generally consumes less time than white-bow ones. Once the model is built, the simulation also take minutes with black-box models compared to days with white-box ones, with the possibility to even outperform the white-box models [37]. The role of these two different types of models is therefore complementary, and not competing. While physical models can be used in the phase of the project of buildings, and to assess the consequences of possible buildings modifications, data-driven models, such as neural networks, should be used for the on-line control of building management systems.

Grey-box models are a mix of the two above. They use input/output data as well as some a priori knowledge on the system with simplified physical representations. A popular grey-box model is the equivalent resistance and capacitance (RC) networks, based on the electric analogy to model the thermal masses and losses with a network of resistances and capacitors. As in the electric RC network, the number of capacitors decides the order of the dynamic system; and similarly, the research findings of RC networks as well as linear systems can therefore be transplanted in the building system for analysis and controller design. This type of model appears to be the most widely applied in the literature [38–41]. Comparing with the white-box model, the grey-box model is less complex, therefore requires much less computation power and can be easily implemented in the real-time control application.

2.3 Control strategies in thermostatically controlled loads (TCLs)

This chapter will focus on control strategies applied in thermostatically controlled loads such as TES and HVAC units as these devices have the highest potential to provide energy flexibility in buildings.

Controls can be divided into two main groups based on the level of control. A local control is present at a single component level, while a supervisory control is responsible for the control of multiple devices as a system. The supervisory controller makes sure that the overall operation of the system is smooth and archive its objective e.g. peak shaving, minimizing cost or maximizing self consumption. The local controller only responsible to keep the process stable while the set-point is kept at all times set by the supervisory controller [42]. Controllers can be categorized into further groups but there is no common terminology in the literature. They are usually divided into soft, hard and hybrid control.

Naidu et al. [42] places the classical controls into the group of hard controls, while Afram et al. [43] treats classical controls as a distinct group. Dounis et al. [44] on the other hand only distinguish between classical, optimal, predictive and adaptive controllers.

Classical control includes the most commonly used control techniques, such as on-off control and PID control. An on-off controller, also called bang-bang or hysteresis controller regulates a process within a predefined lower and upper threshold so that the process stays within these boundaries. These controllers may be realized in terms of any element that provides hysteresis. Most common residential thermostats and hot water tanks currently use bang–bang controllers. PID controllers modulate a controlled variable by using error dynamics, so that accurate control is achieved. There are subgroups of PID controller based on the terms used such as P for solely proportional controller or PI for proportional and integral. Research related to PID controllers focuses on auto-tuning or optimal tuning methods of these controllers, as usually manual tuning is required which can be laborious. PID controllers only perform well, if the operating conditions are similar to the tuning ones [43]. To improve the stability of the controller, gain-scheduling can be implemented with the cost of increasing controller complexity [45].

Hard controllers are based on the theory of nonlinear control, robust control, optimal control, adaptive control and model predictive control (MPC), and are widely used in control system design as local control, even though MPC can be also used for supervisory control. Nonlinear control is effective, but requires a rather complex mathematical analysis when designing the controller as well as an identification of stable states. Optimal and robust control can handle time-varying parameters and disturbances, but robustness is difficult to obtain because of time varying conditions for HVAC systems in buildings. According to Afram et al. specification of additional parameters is required for hard controllers and thus an integration in HVAC systems may be difficult or impractical [43].

Soft controls are mainly used for supervisory control, and based on fuzzy logic neural networks or genetic algorithms. Soft controllers are not very common in real building applications. Neural-network-based control systems need an extensive amount of historical data for training purposes, in order to cover a wide range of operating conditions. Similarly, fuzzy logic controllers require an extensive knowledge of the building operation under different conditions [43].

Hybrid controls are a combination of hard and soft control techniques.

Some of the main challenges facing a HVAC system are non-linear dynamics, time-varying dynamics, time-varying disturbances and supervisory control. MPC is a control method that overcomes these problems. The main features of MPC are summarized in [43]:

- MPC is not a corrective control, but anticipates future system evolution
- An integrated disturbance model can handle disturbances in an explicit manner
- It has the ability to explicitly handle uncertainties and constraints
- It is capable of dealing with processes with time delays
- Energy saving strategies can be integrated in the controller formulation
- Multiple objectives can be achieved by using appropriate formulations of the cost function

- MPC can be used for supervisory as well as local control
- Explicitly includes the prediction of occupant behaviour, equipment use and weather forecasting

The research on MPC has intensified during the last decade. It has been proved that this control method can achieve energy savings while maintaining or even improving comfort levels in buildings. Researchers show different approaches for applying MPC for controlling HVAC systems in buildings in combination with thermal energy storages in order to deploy the demand side flexibility that a building may offer.

Reinforcement learning (RL) based controllers have shown remarkable progress recently in achieving state of the art results in many difficult and previously unsolvable domains [46–48]. Some pioneering work on the suitability of applying RL methods to building control appeared in [49]. However much of these research used primitive RL algorithms such as Q-learning and SARSA [50–52], that have several limitations which has been addressed in the most recently developed algorithms since then. Very recently, some studies have started to appear where advanced RL controllers are applied to building control [51, 53]. RL control approaches the same problems differently than MPC, and these differences can be better explained dividing the RL algorithms into further two categories: model-free and model-based RL.

Model-free RL as the name describes does not based on a system dynamics model in opposition to MPC. It also does not have the capability to learn these dynamics, but it directly learns the optimal control strategy based on its interactions with the system. The working principle of these algorithms can be described as follows: the agent observes the state of the system, then takes an action and observes its reward (or penalty) from the environment. Based on these reward the agent is able to update its policy, thus learning the optimal actions to maximise its reward stream. By designing the rewards the controller can be optimized for any objective function.

Model-based RL similarly to the MPC is based on a system dynamics model. The controller in addition to the reward function in model-free ones also learns a transition model through supervised learning. Based on these functions the controller is able to optimize its actions to maximize its reward. These algorithms can perform as well as MPC while also offering the potential to greatly reduce computational complexity. As RL is able to learn the policy after a state was observed, MPC calculates the optimal action every time it revisits the same state. [54]

2.4 Introduction to the used machine learning model

Machine learning algorithms find natural patterns in data that generate insight and help make better decisions and predictions. They are used every day to make critical decisions in medical diagnosis, stock trading, energy load forecasting, and more. Machine learning in usually divided into two types. Predictive or supervised and descriptive or unsupervised learning.

The aim of supervised machine learning is to build a model that makes predictions based on evidence in the presence of uncertainty. A supervised learning algorithm takes a known set of input data (features, attributes or covariates) and known responses to the data (output or response variable) and trains a model to generate reasonable predictions

for the response to new data. Supervised learning uses classification and regression techniques to develop predictive models. When the output is categorical, e.g. whether an email is genuine or spam, or whether a tumour is malignant or benign the problem is known as classification or pattern recognition. When the response variable is continuous, the problem is known as regression, e.g. changes in temperature or fluctuations in power demand.

Unsupervised learning finds hidden patterns or intrinsic structures in data. It is used to draw inferences from datasets consisting of input data without labeled responses. Clustering is the most common unsupervised learning technique. It is used for exploratory data analysis to find hidden patterns or groupings in data. This is a much less well-defined problem, since we are not told what kinds of patterns to look for, and there is no obvious error metric to use.

There is a third type of machine learning, known as reinforcement learning which is more and more common in recent years. This is useful for learning how to interact with the environment based on occasional reward and punishment signals.

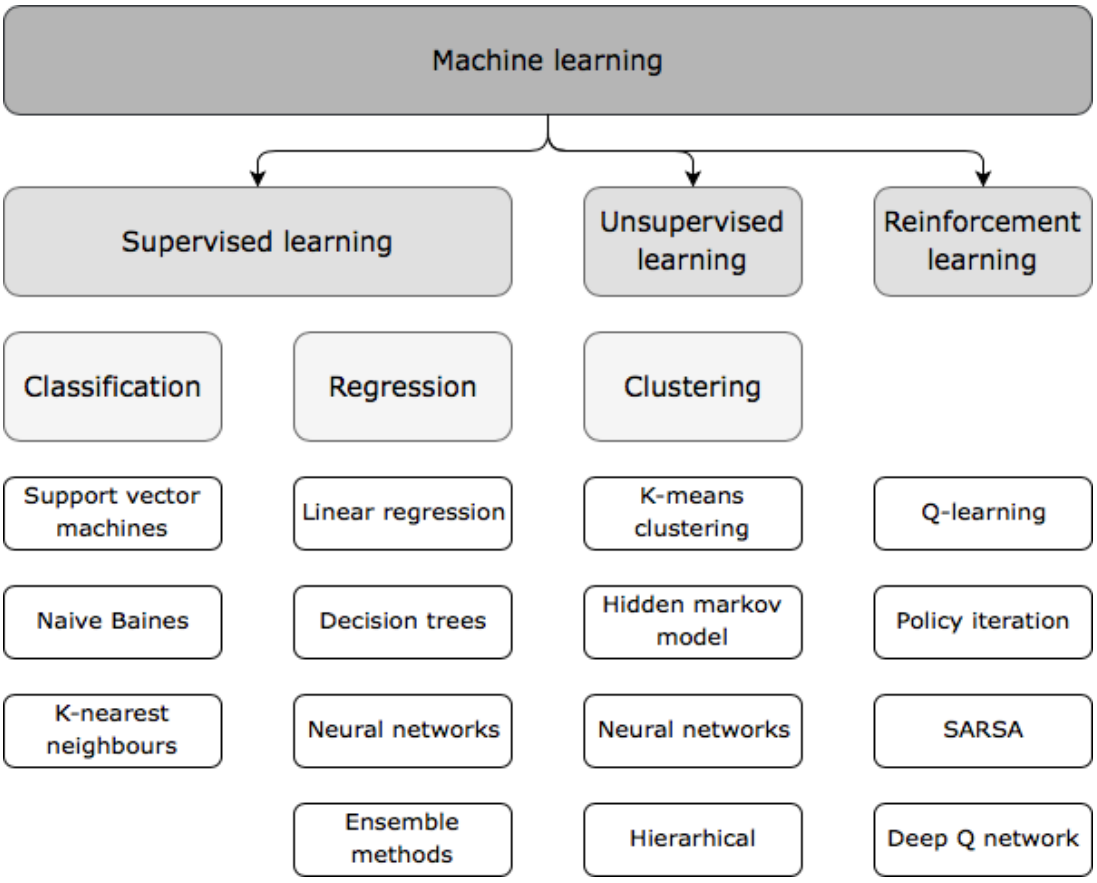

FIGURE 2.2: Examples of algorithms for different types of machine learning

There are numerous different algorithms for each type of machine learning. However the so called "no free lunch theorem" [55] states, that there is no single best algorithm that works optimally for all kinds of problems. Algorithm selection depends on the size and type of data, the insights you want to get from the data, and how those insights will be used. Figure 2.2 lists a few example algorithms for each machine learning type [56].

2.4.1 Neural networks (NN)

In its most general form, a neural network is a machine that is designed to model the way in which the brain performs a particular task or function of interest. It is a massively parallel distributed processor made up of simple processor units (neurons), which has a natural propensity for storing experiential knowledge and making it available for use. it resembles the brain in two respects:

1. Knowledge is acquired by the network from its environment through a learning process.

2. Interneuron connection strengths, known as synaptic weights, are used to store the acquired knowledge.

The procedure used to perform the learning process is called learning algorithm, the function of which is to modify the synaptic weights of the network in an orderly fashion to attain a desired design objective [57].

2.4.2 Multilayer perceptrons (MLP)

Multilayer perceptrons are the most popular type of neural networks in use today. They belong to a general class of structures called feedforward neural networks, a basic type of neural network capable of approximating generic classes of functions, including continuous and integrable functions.

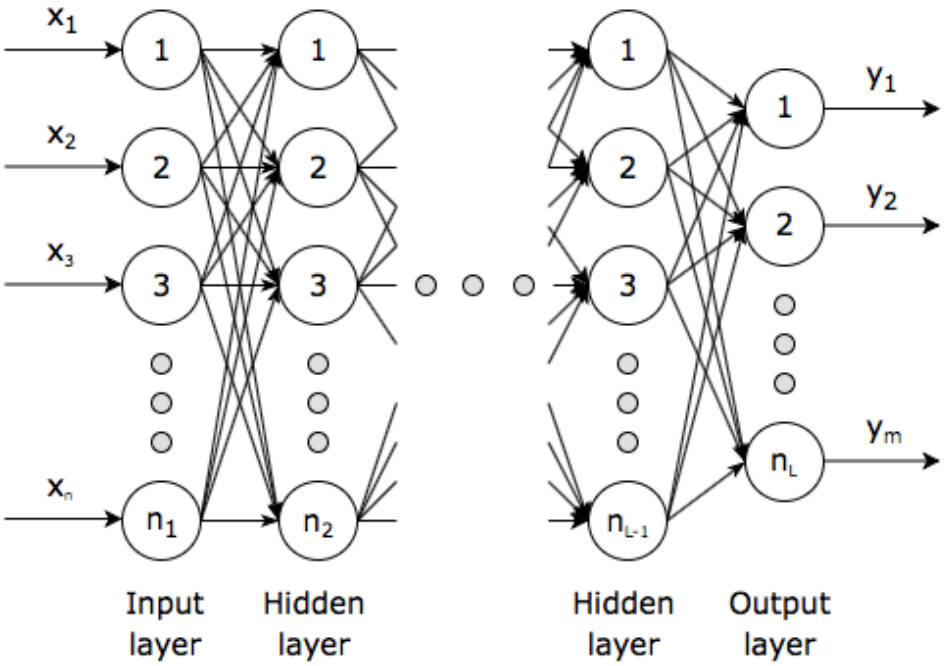

FIGURE 2.3: MLP structure

In the MLP structure, the neurons are grouped into layers. The first layer called the *input* and the last the *output layer*, because they represent the inputs and outputs of the overall network. There are as many neurons in the input layer as input features, while the number of neurons in the output layer matches the number of response variable of

the model. The remaining layers are called *hidden layers* [58]. A typical MLP structure is shown in figure 2.3.

In a NN, each neuron with the exception of the neurons in the input layer receives and processes the input from other neurons, then passes the information to the output end of the neuron. The inputs from the previous layer are first multiplied by the corresponding weights, and the resulting products are added to produce a weighted sum, which is passed through an *activation function* to produce the final output of the neuron, also the input for the neurons in the next layer. There are multiple different activation functions, but a few most commonly used are e.g. sigmoid, hyperbolic-tangent, rectified linear unit activation functions [59].

The main objective is to find an optimal set of weight parameters, such that the output of the NN closely resembles the original behaviour. This process called training which requires a training set where the inputs and the outputs are known and the used algorithm is called back propagation (BP). This algorithm consists of two steps. After *initialising* the weight parameters, the forward error is calculated which is the difference between the target and the predicted values. The difference also known as the error is determined by a *loss function*. During the second step, the weights are updated by the negative gradient of the error multiplied by a parameter called *learning rate*.

In order to evaluate the performance of the model, the loss function is necessary but not sufficient. There are two phenomena, which called overfitting and underfitting. Overfitting happens when the weights are set to match precisely the outputs of the training data, but performs worse on a new set of data other than the training set. Underfitting is the opposite phenomenon, whereby the model is unable to capture the trends in the data. The structure of the NN can be one of the cause of these phenomena. If there is inadequate number of layers, or neurons in the layers, the NN will be unable to capture the complexity of the problem. On the other hand, if there are too many of them, the NN will be prone to overfitting. In order to identify these phenomena the available dataset is split into two parts, a training and a test set.

The performance of the NN highly depends on not just the parameters of the architecture, but also on a set of parameters, which are chosen before the training, called hyperparameters. The definitions of the used hyperparameters in this thesis is listed below.

- **initialiser**: determines the weight initialization scheme, therefore the starting weight parameters of the network
- **activation function**: a nonlinear function, which determines the final output of the node, and gives the nonlinear capacities of the NN
- **reguliser**: gives an extra term in the loss function to penalise high weigh values in order to prevent overfitting. It can be L1, L2 norm, or a combination of them.
- **loss function**: also called cost function is the way to determine the inconsistency between the real output values and the predicted values.
- **optimizer**: the optimization function is responsible for updating the weights during back propagation. There are fixed learning rate algorithms and adaptive learning rate ones.

- **learning rate**: defines the rate the weights are updated at each back propagation.
- **momentum**: determines the velocity with which the learning rate has to be increased as the minima is approached.
- **epochs**: is the number of times the whole training dataset is shown to the network during the training process.
- **batch size**: is the number of samples given to the network after each parameter update.

Optimising all of the architecture parameters and hyperparameters is a challenging task on its own. There are different ways to optimize them, e.g. random search, manual search, grid search, bayesian optimization.

Chapter 3

Methodology

This chapter explains the steps and calculations made throughout this thesis in detail to acquire the results shown in later chapters.

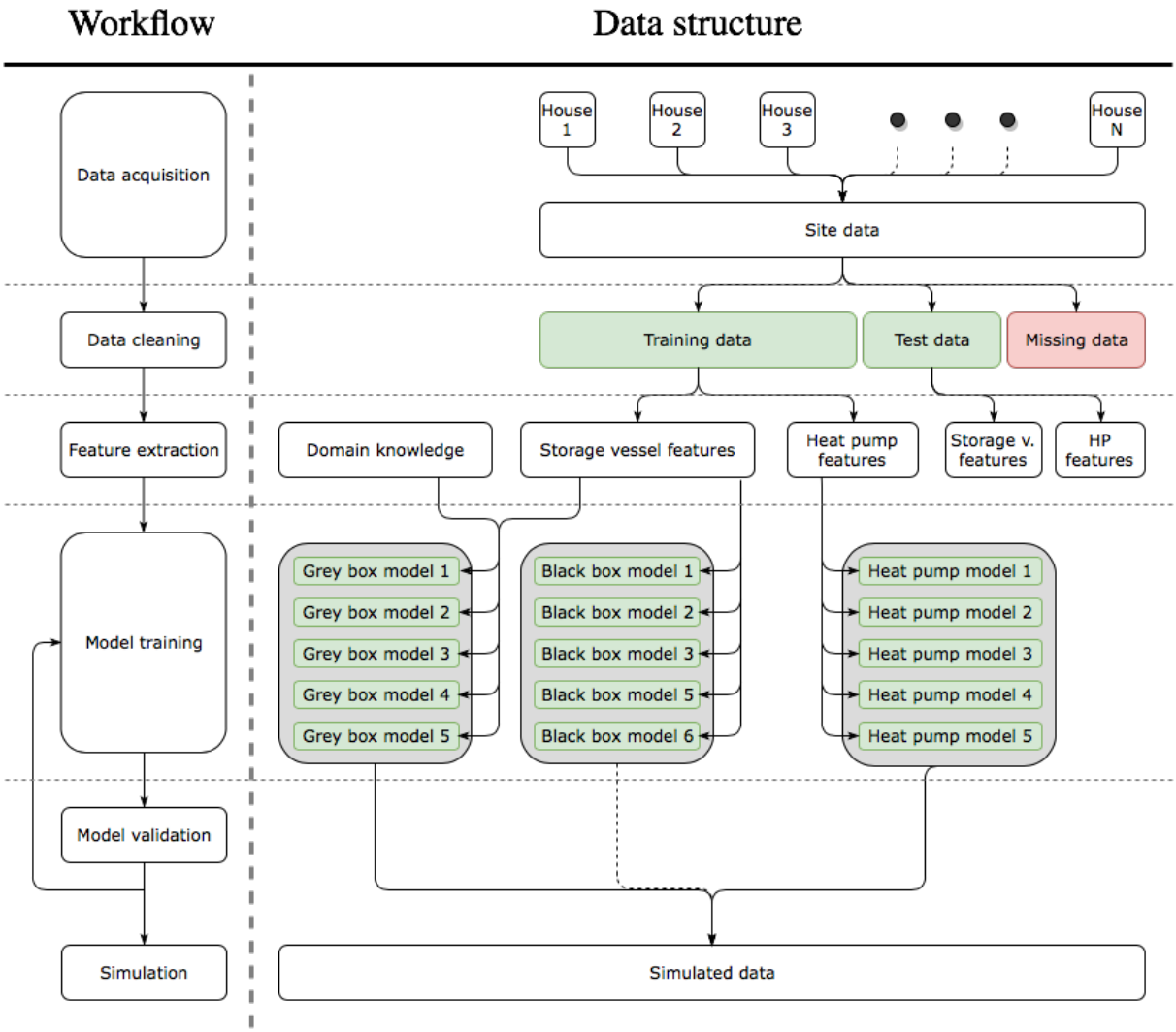

FIGURE 3.1: Workflow and data structure of this thesis

Figure 3.1 visualizes the workflow followed for each site. At the start N number of houses are given, with the same structure and equipment. Based on the assumption that the thermostatically controlled loads behave similarly given that the structure of the

surroundings and the conditions are similar, the data collected individually from these houses can be treated as one. Following the data collection, any faulty or missing data is removed from the dataset. This cleaned data is then split into two sets, a training and a test set. The former is used for model training, while the latter is for model validation. So called features are extracted from the cleaned data to form the input of the models. Using these features a given number of models are trained. During validating the unsuccessfully trained models are filtered out and replaced with a newly trained ones, until the required number of models is reached (Fig. 3.1 black box n.4 is replaced with black box n.6) . These models can be later used for e.g. modelling, forecasting, control or simulation. The steps in the workflow are detailed below chapter by chapter.

3.1 Data acquisition

The data used in this thesis was collected through Enervalis' [60] smart building platform from multiple houses with identical sensor setup shown in figure 3.2.

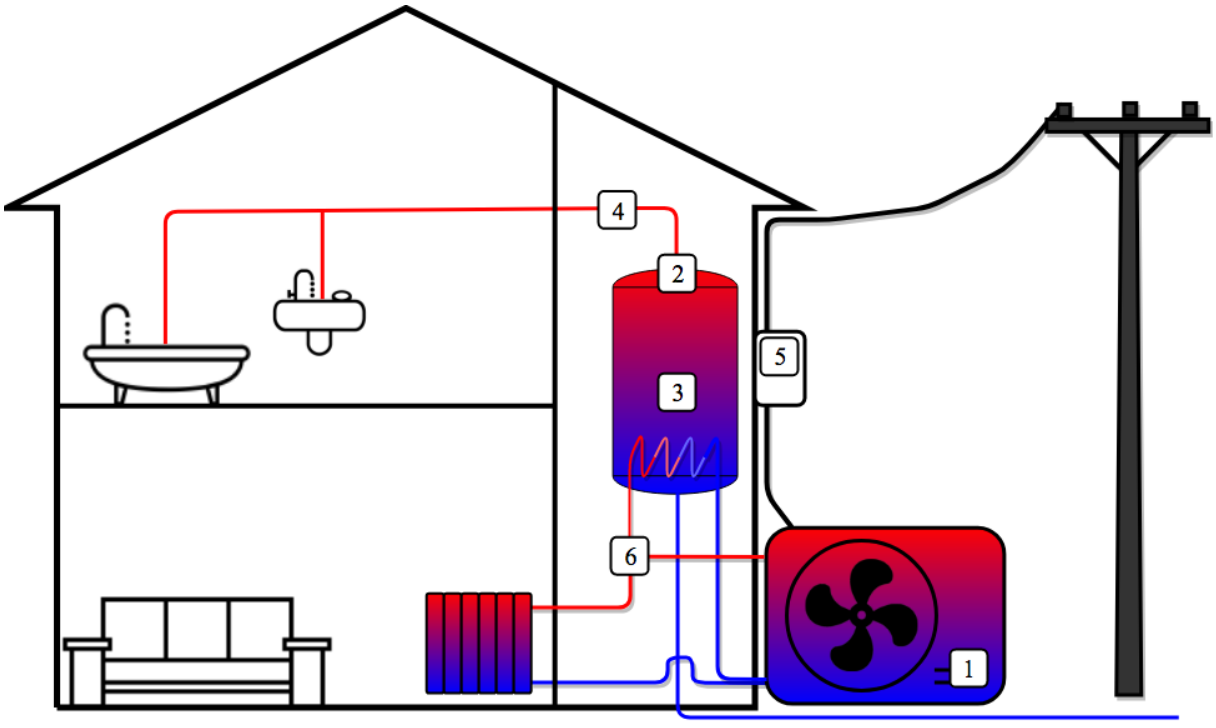

FIGURE 3.2: Sensor setup present in each house on all sites
1. Outside temperature, 2-3. Water temperature at the outflow and in the tank, 4. Flow meter, 5. Smart meter, 6. Heat pump operation mode

All of the houses use a heat pump (HP) for domestic hot water (DHW) production and space heating as well with two separate circuits, but the HP can only reheat one of these circuits at a time. The HP records the operational mode (6) and includes a temperature sensor, which measures the ambient temperature. A commercial hot water storage vessel is used, which includes a flow meter (4) and a temperature sensor (3) inside the tank, used for the internal reheat control. In some of the houses an additional temperature sensor was installed non-invasively onto the outflow pipe of the tank in order to validate the performed improvements. All of the houses are equipped with a smart meter (5), which

is responsible to measure the power uptake of the HP.
The following data is collected from the sensors:

- Time of the observation
- T_{out} (1): Outside temperature [°C]
- T_{top} (2): Water temperature at the top of the vessel [1] [°C]
- T_{mid} (3): Water temperature inside vessel [°C]
- Q (4): DHW consumption through flow meter [L/h]
- P (5): Power output of the heat pump [W]
- HP_{mode} (6): HP's operation mode

The heat pump's operation modes are represented by the following numbers:

- 0: Idle
- 1: DHW production
- 2, 5: Space heating
- 6: Legionella cycle [2]

Figure 3.3 shows a one day long subset of data from a single house. Due to the thermodynamic losses in the hot water tank, and the consumption of DHW (Q), which is replaced by an approximately 15-20 °C water from the grid, the water temperature in the tank (T_{mid}) is decreasing until 10:30. As the T_{mid} drops below the internal threshold ($T_{threshold}$) the HP switches into DHW production mode (mode 1), therefore the consumption (P) increases, until the T_{mid} does not reaches the $T_{setpoint} = 55\,°C$. A few things are important to mention. First, the built-in sensor of the DHW vessel is able to measure the temperature only at a single height. Due to thermal stratification in the water tank there is a temperature difference along the height of the vessel, which is caused by the difference in thermal buoyancy [61]. This limitation of one sensor lets the system reheats itself, even though the outflow water temperature might be above the $T_{threshold}$ at the top of the vessel. Secondly, the measured temperature by the top sensor is highly influenced by the ambient temperature when there is no water-flow in the pipe. This is due to the non-invasive installation of the sensor.

3.2 Data cleaning

From the measurement on site until the recording in the database at a server, the data is passed through multiple devices during the process. This implies that if any of these devices malfunction the data is lost. Figure 3.4 illustrate an example where the data was lost and filled with interpolated data by the platform. There are multiple signs,

[1] only in houses where sensor is installed
[2] which prevents the development of legionella bacteria in the water tank by reheating the water to 65 °C

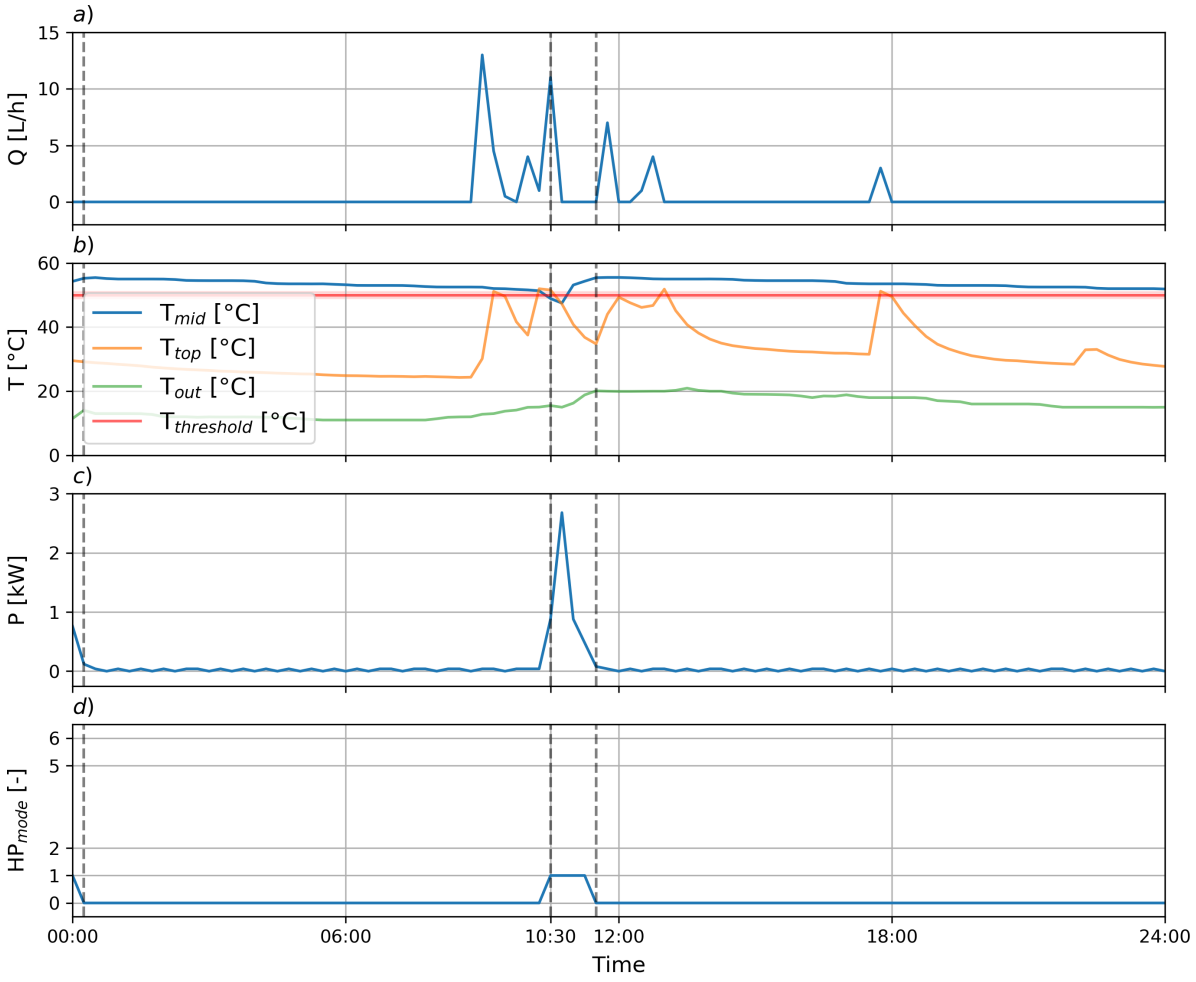

FIGURE 3.3: Sample of collected data
a) DHW consumption, b) Data from temperature sensors, c) HP's power consumption, d) HP's operation mode

that indicate wrong data collection. First of all, all the temperature values stay almost completely flat, despite high water consumption peaks and non-zero power consumption values. Secondly, the HP_{mode} stays 0 (idle) even though the power consumption is non-zero after 12:00.

It is very important that these periods, where data is missing are removed from the dataset before further processing and calculations, as they can highly influence the performance and accuracy of the later introduced models.

3.3 Feature extraction

The hot water tank is periodical and constantly switches between two states: discharging and reheating. During the discharge period, the tank looses its energy due to hot water consumption and heat losses. During a reheat period, the tank is reheated by a heating element, in the case of the vessels used in this thesis, by an external heat pump unit. Therefore to fully model the behaviour of the hot water tank it is divided into two parts,

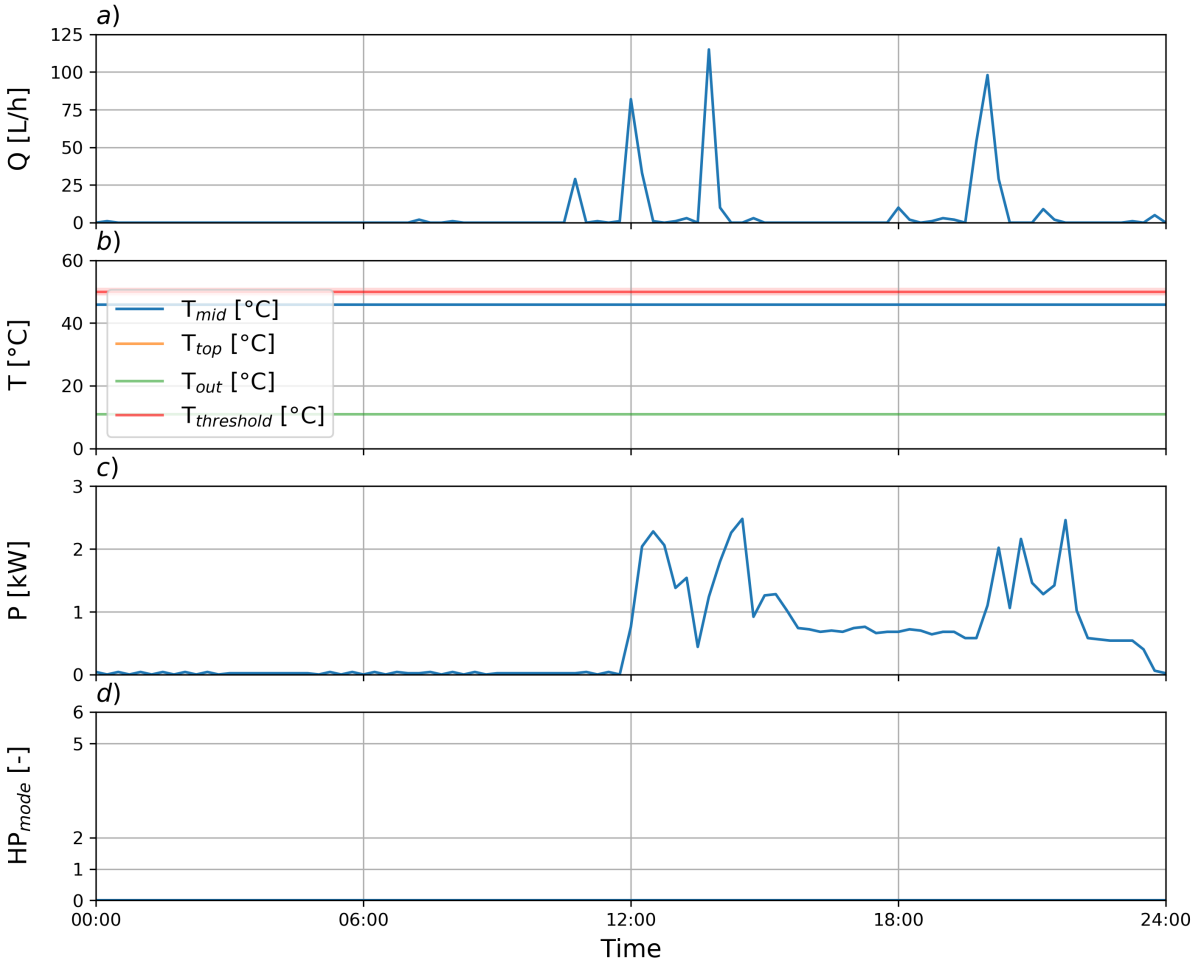

FIGURE 3.4: Example of missing data
a) DHW consumption, b) Data from temperature sensors, c) HP's power consumption, d) HP's operation mode

discharge and reheat cycles and from now referred to as storage vessel model and heat pump model respectively.

3.3.1 Features of storage vessel model

In order to create a model that is able to predict the temperature at the midpoint T_{mid} from the sensor data, we formulate the function approximation problem as equation 3.1:

$$y = f(x_1, ...x_n), \quad \text{where} \quad y = T_{mid} \quad \text{and} \quad x_1, ..., x_n = \textit{the input features} \tag{3.1}$$

Much research has been done in building black box modelling by simply taking time series data and use it directly as input features. Dimensionality reduction (e.g. PCA, autoencoders) is another common alternative to use on time series data, with very limited interpretability. To retain interpretability, feature engineering is used in this thesis and following input features are extracted from the dataset:

1. T_{reheat}, water at the start of the discharge cycle measured by sensor 3 [°C]

2. $V_0 + V$, total water consumption since the start of the discharge cycle plus water volume between the outflow and the temperature sensor (sensor 3) [L]

3. t, time passed since the start of the discharge cycle [h]

The output or target is defined as:

- T_{mid}, water temperature measured by sensor 3 [°C]

t_0 is the start of the discharge cycle, which is defined as the time when the HP_{mode} switches from mode 1 or 6 to a mode which does not affect DHW temperature[3]. In order to incorporate the sensor's position, which can vary between tanks, we define V_0 as the water volume between the sensor's position and the outflow of the vessel.

During normal operation the hot water tank operates between the set-point ($T_{setpoint}$) and the threshold temperature ($T_{threshold}$). This range is in most of the cases not larger than 5-10 °C.
In order to improve the model performance, domain knowledge can be integrated in the form of features. In this case it can be assumed that the water temperature will become equal to the inflow water temperature without a reheat cycle, if the water consumption is greater than the capacity of the vessel. Therefore the initial hot water from the tank is fully exchanged by fresh water from the water grid. This can be formulated as features:

$$if \quad V > V_{vessel}, \quad then: \quad T_{mid} = T_{inflow} = 15\,°\mathrm{C}$$

This assumption is valid for any T_{reheat} reheat temperature and any t_{hist}.

3.3.2 Top temperature sensor

Features were extracted from the top sensors in a similar manner as the discharge cycle. The main difference is that the temperature data is not coming from the sensor inside the vessel (3), but the sensor installed on the top of it (2). As this sensor is placed at the top of the vessel $V_0 = 0\,\mathrm{L}$.
These features were only used for validation purposes, as the goal is to keep the used sensors at a minimum to reduce costs. As seen in figure 3.3, the top sensor is only measuring the correct value if there is a high amount of water flow through the pipe, which lets the pipe equilibrate with the water temperature. Therefore the features are only added if the $Q(t) > 20\,\mathrm{L}$.

3.3.3 Features of heat pump model

We formulate the function approximation problem for the charging model as equation 3.2 where the target is now the amount of energy consumed during a reheat cycle:

$$y = f(x_1, ...x_n), \quad \text{where} \quad y = E \quad \text{and} \quad x_1, ..., x_n = \textit{the input features} \tag{3.2}$$

The required energy to reheat the tank depends on many factors. First of all, it depends on the state of the tank at the beginning of the reheat. This is represented with the last features of the previous discharge cycle. Secondly, it depends on water temperatures at

[3] mode: 0, 2 or 5

the start and at the end of the reheat cycle. Furthermore, water consumption during the reheat cycle further increases the required energy, as it removes heat from the tank and works agains the reheat element. Last but not least, the outside temperature also has impact on the heat pump's efficiency, thus the required reheat amount.

The legionella cycle (mode 6) is neglected in our charge model, as the reheating behaviour is substantially different from the regular reheat cycle.
The t_0 is still defined as the start of the previous discharge cycle, while t_r is defined as the time when the heat pump mode switches to 1 for the first time from a mode which does not influence the water temperature[3].

The above mentioned factors are formulated as features:

1. T_{reheat}, the midpoint temperature at the start of the previous discharge cycle [°C]
2. V_{dc}, total water consumption during the previous discharge cycle [L]
3. t, length of the previous discharge cycle [h]
4. T_{start}, water temperature at the start of the reheat cycle recorded by sensor 3 [°C]
5. T_{end}, water temperature at the end of the reheat cycle recorded by sensor 3 [°C]
6. V_c, total water consumption during the reheat cycle [L]
7. $\overline{T}_{out}$, outside temperature during the reheat cycle [°C]

The target is defined as:

- E, total energy consumption during the reheat cycle [Wh]

3.4 Machine learning models

3.4.1 Model training

As mentioned above, three different model types were trained (Figure 3.5).

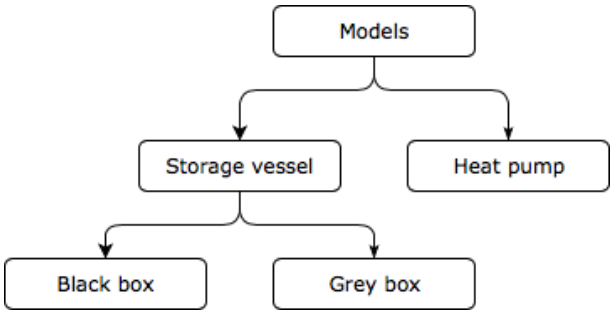

FIGURE 3.5: Trained model types

- Heat pump model: trained on the heat pump features created from the training set
- Black box storage vessel model: trained only on the storage vessel features extracted from the training set
- Grey box storage vessel model: trained on the extracted features as with the black box model, together with the features created to incorporate domain knowledge

The same Multilayer Perceptron (MLP) type Neural Network (NN) was used for all three types of models, built with the Keras [62] package in Python [63]. The structure of this NN is shown in table 3.1.

TABLE 3.1: Structure of the used Neural Network

Layer	Type	Neurons
1	*Input*	$n_{inputfeatures}$
2	*Hidden*	1000
3	*Hidden*	500
4	*Hidden*	150
5	*Hidden*	100
6	*Output*	1

The hyperparameters listed in table 3.2 were chosen after a grid search. As not just the number of features but also the number of datapoints vary between the storage vessel and heat pump models, some hyperparameter values are different, but identical in both black box and grey box models. The kernels were initialized with he_{normal} initializer, [64] and an *L2 regularization* was added to each layer. The *selu* activation function was applied for all layers [65] and *Adam* [66] algorithm was utilized to minimize the mean absolute error. Initial learning rates were 0.01 which was reduced until 0.001 with the reduce learning rate on plateau callback. An early stopping callback was also implemented with the patience set to 50 % of the epochs.

TABLE 3.2: Used hyperparameter values for storage vessel (black box and grey box) and heat pump models

Hyperparameter	Storage vessel	Heat pump
Initializer	he_{normal}	he_{normal}
L2 Regulizer	0.01	0.05
Activation function	Selu	Selu
Loss function	mean absolute error	mean absolute error
Optimizer	Adam	Adam
Batch size	128	32
Learning rate	0.01	0.01
Epochs	50	200

3.4.2 Model validation

The goal of the validation step is to qualitatively and quantitatively qualify the trained models. The function of the loss during training serves with a lot of information about the quality of the model and helps to identify if the model is under or overfitting.

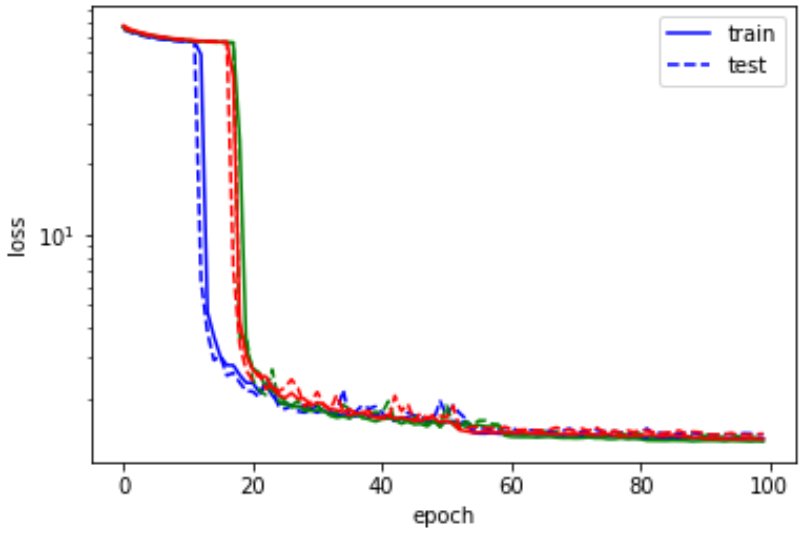

FIGURE 3.6: Loss function on the training and test set of three models (blue, red, green) during training

Figure 3.6 shows the value of the loss function for the training and the test sets during the 100 epoch long training cycle for 3 models with different colors. As the loss stopped to decrease significantly and converges to the same value in all 3 cases the models can be qualified as successfully trained. As the loss on the test set is very close to the loss on the training set, the models are neither over- nor under-fit.

The successfully trained models are collected to form an ensemble for forecasting. This means that the individual models predictions are collected separately and the distribution of the predictions is used for forecasting instead of an individual model's prediction. This make it possible to quantify the certainty of the prediction by using the mean of the

distribution as the prediction and the standard deviation as prediction interval. Figure 3.7 displays the real midpoint temperature during one discharge cycle as well as the predictions with mean and prediction interval.

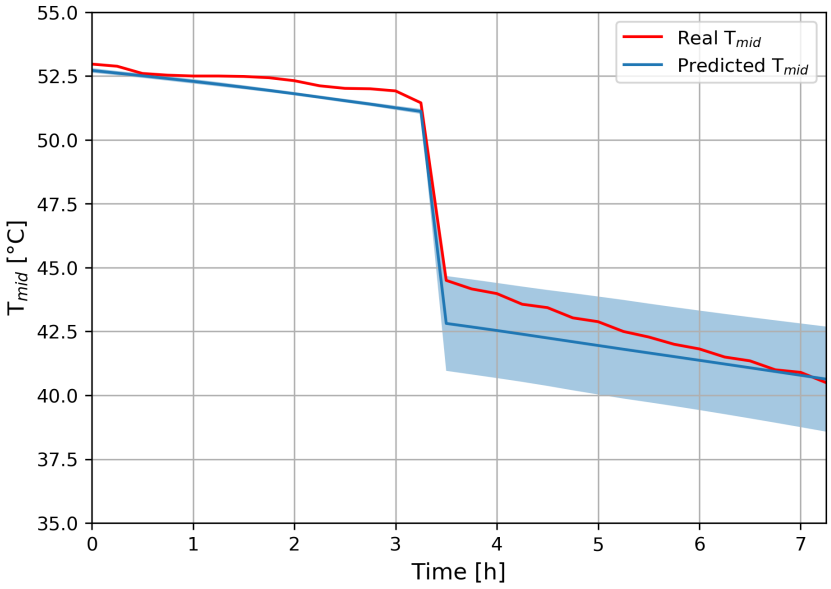

FIGURE 3.7: Real and predicted midpoint temperatures during a discharge cycle with prediction interval

3.4.3 Model prediction

In order to predict the temperature distribution in the whole water tank from only one sensor in the middle, based on the assumption that the water flow is always laminar in the tank, the following assumption is made:

$$T_v(T_{reheat}, V, t) = T_{V_0}(T_{reheat}, V + (v - V_0), t),\ where: \tag{3.3}$$

- T_v: temperature at volume v from the top of the vessel [°C]
- T_{reheat}: initial temperature of the discharge cycle[4] [°C]
- V: water consumption since the start of the discharge cycle [L]
- t: time passed since the start of the cycle [h]
- V_0: location of the sensor [L]

With this assumption the predicted water temperature distribution look likes in figure 3.8. In this way it is possible to predict the temperatures above the sensor, limited by the water consumption during the discharge cycle.

[4] at sensor height

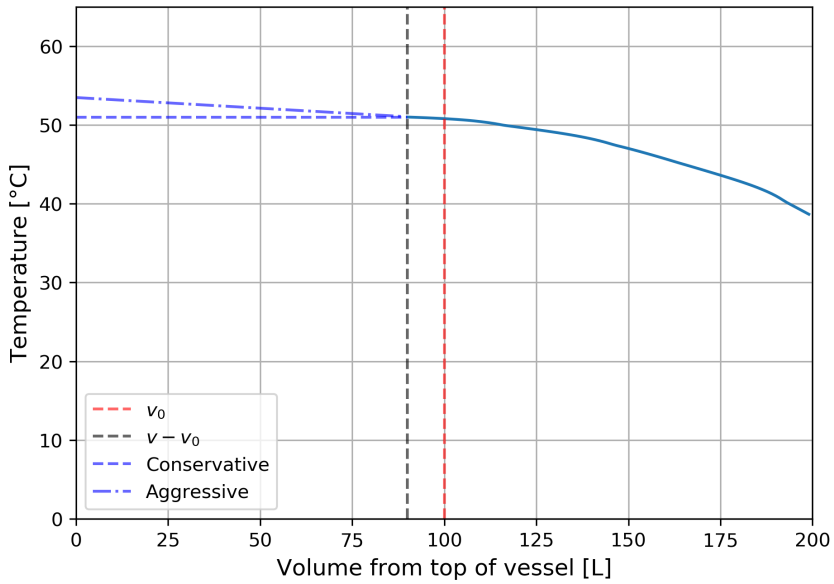

FIGURE 3.8: Predicted water temperature distribution by one model from equation 3.3 with solid blue line, aggressive and conservative assumption with dotted and dashed blue lines. Sensor position and the end of prediction zone with red and black dashed lines respectively.

With the assumption that the temperature is monotonously non increasing function of the volume from the top, conservatively the temperature above our prediction can be assumed to be equal to the highest temperature. With a more aggressive assumption the top of the vessel can be modelled with linear regression, fitted onto the first n points of the prediction. During this work all the prediction used a linear prediction using 20 *points*.

3.5 Water tank simulator

The above described storage vessel and heat pump ensembles were used to create a simulator of a hot water tank. The simulator takes in the following inputs:

- Q(t): Water consumption profile during the simulation period [L/h]
- T_{out}(t): Outside temperature during the simulation [°C]
- $T_{mid}(t_0)$, $T_{reheat}(t_0)$: initial midpoint and reheat temperature [°C]
- n storage vessel models
- n heat pump models
- heat pump control mode

The flow chart of the simulation is shown in figure 3.9. Based on the inputs, the controller switches into either reheat mode (mode 1) or idle (mode 0). If the HP is idle, the midpoint temperature is predicted by the storage vessel models and the time is incremented. As the tank is being emptied, the controller eventually switches into mode 1 and the

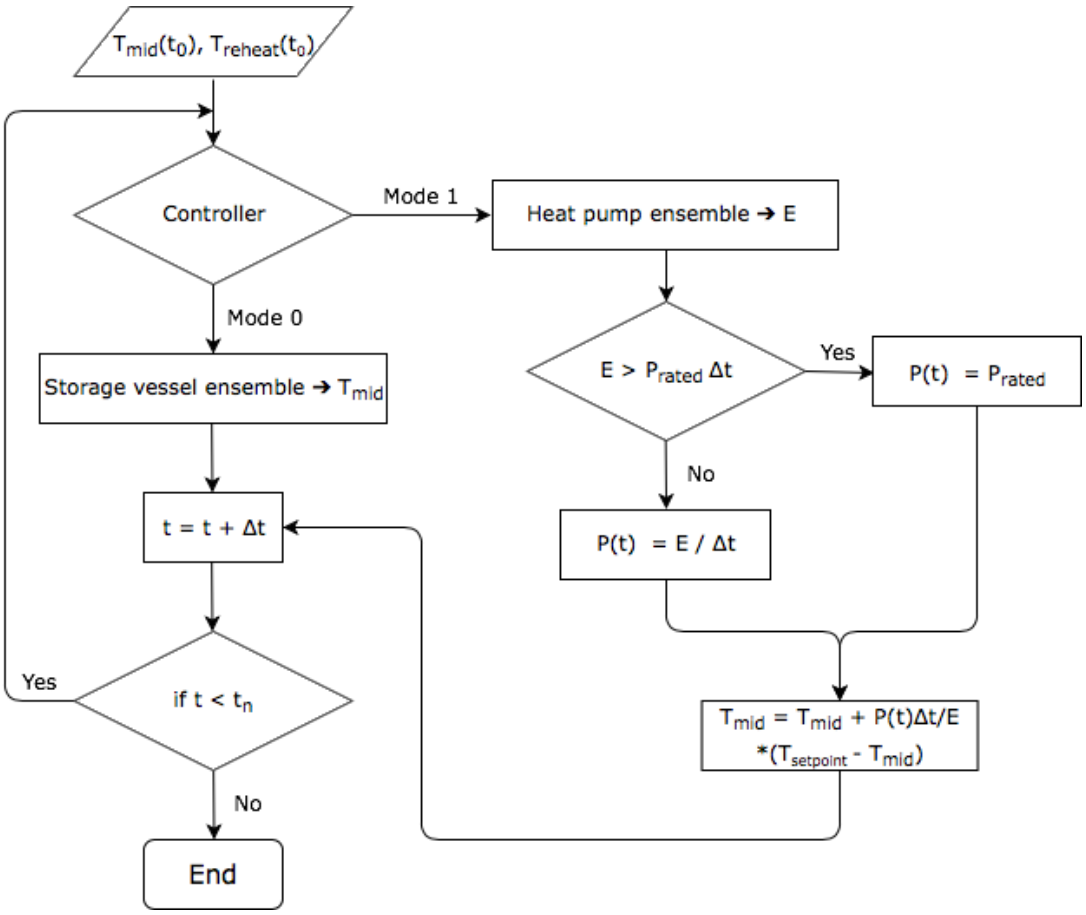

FIGURE 3.9: Flow chart of simulation

amount of energy to reheat (E) is predicted by the heat pump ensemble. If the energy is higher than the HP's rated power multiplied by the delta time between steps, the power consumption is the HP's rated power, otherwise it is defined by E. During reheat, the midpoint temperature increase is modelled linearly with the power output. The loop is repeated until the defined simulation length (t_n).

3.5.1 Rule based controller

To simulate the original controller of the heat pumps, a rule based controller (RBC) was implemented as shown in figure 3.10. The controller is designed to keep the temperature between the upper ($T_{setpoint}$) and the lower ($T_{threshold}$) temperature bounds. As the temperature drops below the $T_{threshold}$ the heat pump switches into mode 1 and start reheating the water. The controller only exits mode 1 when the temperature reaches or exceeds the $T_{setpoint}$.

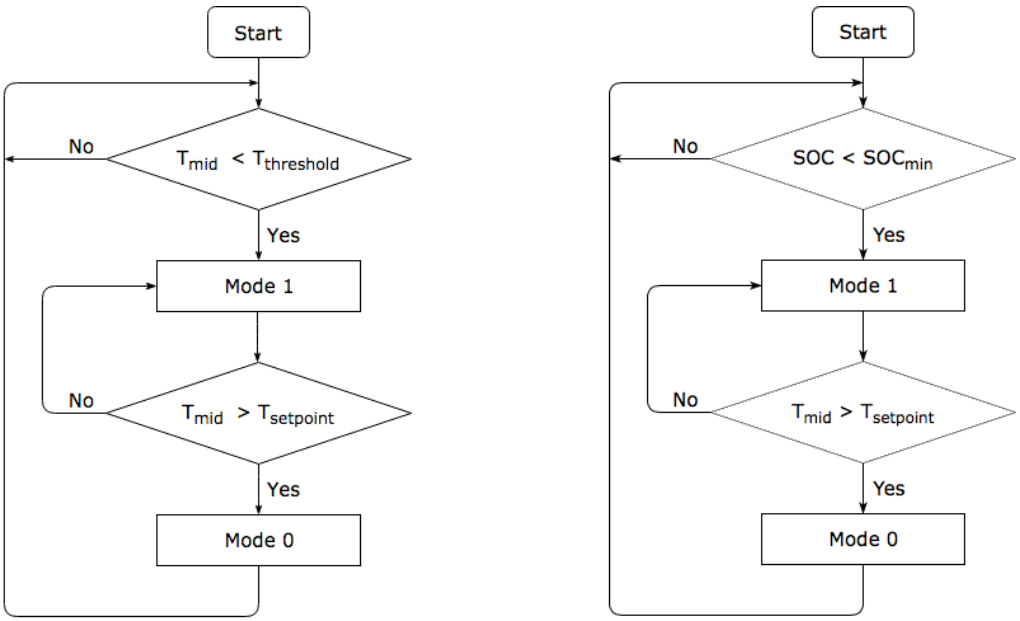

FIGURE 3.10: Control logic of rule based controller (left) and energy efficient controller (right)

3.5.2 Energy efficient controller

The energy efficient controller is identical to the RBC in control flow, but the control variable is different (Fig. 3.10 right). Instead of using a single midpoint temperature, the controller uses the state of charge (SOC) as the control variable. The SOC can be defined as the amount of water which is above the $T_{threshold}$, demonstrated in figure 3.11.

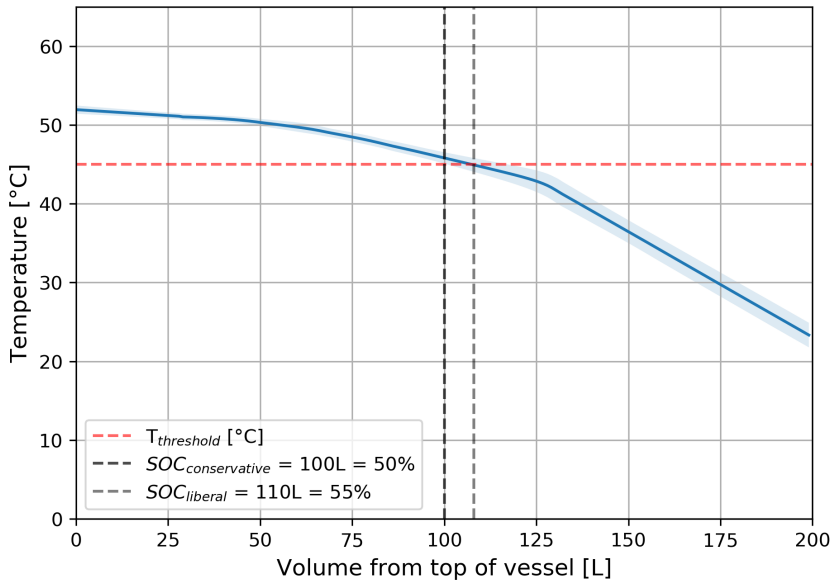

FIGURE 3.11: Water temperature profile in the vessel with state of charge for a given threshold temperature

The minimum allowed SOC, which triggers the energy efficient controller to reheat is from now on referred to as *safety net*, given in liters or percentage of tank capacity.

A known water temperature profile allows to leave the assumption that the water temperature in the hot water tank is unified. In stratified tanks, this means that the energy content of the tank is modelled better therefore better controllable.
While a single sensor would initiate reheat in figure 3.11, the energy efficient controller will initiate the reheat when the SOC_{min} is reached. If the $SOC_{min} < V_0$ the energy efficient controller is expected to reheat less often than the RBC. The state of charge is in this case conservatively 100 L or 50 %, where the prediction interval reaches below the $T_{threshold}$. In a more aggressive or liberal estimation the SOC would be around 110 L or 55 %, where the mean of the prediction drops below the threshold value.

3.5.3 Controller performance

In order to evaluate the controller performance, two things were taken into consideration: energy saving potential (S) and occupant comfort (C). Energy saving potential was calculated as the relative difference compared to the rule-based controller:

$$S = \frac{Q_{rbc} - Q_{ee}}{Q_{rbc}} \tag{3.4}$$

while the occupant comfort was calculated as the fraction of time the state of charge of the hot water storage is above 0, thus the occupant comfort is not violated:

$$C = \frac{1}{n} \sum_{t_0}^{t_n} x \tag{3.5}$$

where:

$$f(x) = \begin{cases} 0, & \text{if } SOC_t = 0 \\ 1, & SOC_t \geq 0 \end{cases}$$

After calculating the results with safety nets ranging from 0 until the the location of the sensor (50 % in case of Site R), the results were scaled, between 0 and 1. This ensures that both objectives weight on a similar scale when calculating the overall controller performance. As these two objectives may have different importance on different sites, the overall controller performance is calculated with a single α parameter as follows:

$$P = \alpha S + (1 - \alpha) C \tag{3.6}$$

This way by changing the α parameter, different weights can be assigned to the two objectives.

3.6 Energy flexibility indicators

Three parameters were calculated as introduced by Reynders et al. [30].

They define the available structural storage capacity for active demand response (C_{ADR} [kWh]) as the amount of heat that can be added to the structural mass of a dwelling, in the timeframe of an ADR event, without jeopardizing thermal comfort.
To quantify the available storage capacity in thermal storages, the amount of energy is forecasted by the heat pump model ensemble to reach the default midpoint temperature.

The available storage capacity is then given by the integral, of the difference between the heating power during this ADR event (Q_{ADR} [W]) and the heating power in normal operation (Q_{Ref} [W]), i.e. the temperature set point equal to the minimum comfort temperature:

$$C_{ADR} = \int_0^{l_{ADR}} (Q_{ADR} - Q_{ref})dt \tag{3.7}$$

The storage efficiency (η_{ADR} [-]) is defined as the fraction of the heat that is stored during the ADR event that can be used subsequently to reduce the heating power needed to maintain thermal comfort. The efficiency is calculated using the same simulations that are used to quantify the storage capacity. Given these simulations, the efficiency is calculated as:

$$\eta_{ADR} = 1 - \frac{\int_0^{\infty} (Q_{ADR} - Q_{ref})dt}{\int_0^{l_{ADR}} (Q_{ADR} - Q_{ref})dt} \tag{3.8}$$

The integral in the denominator is equal to the heat stored in the storage event or the available storage capacity (C_{ADR}). A part of this heat can be used after the ADR event to reduce the heating power needed to maintain occupant comfort. The numerator represents this fraction of the heat stored during the ADR event that is not recovered over a long period.

The power shift (Q_δ [W]) is defined as the difference between the heating power during the ADR event (Q_{ADR} [W]) and the reference heating power (Q_{Ref} [W]) during normal operation. Starting from the building in a current state, the thermal response of the building is activated and the change in the heating power is modelled.

$$Q_\delta = Q_{ADR} - Q_{ref} \tag{3.9}$$

An additional metric, the recovery period was calculated which is defined as the time duration it takes for the storage tank to return to normal operation after an ADR event, thus $Q_\delta = 0$.

Chapter 4

Results

In the scope of this thesis, 3 different sites were investigated. For data privacy reasons the sites will be named as Site A, F and R. For each site the amount of data is collected from n number of houses during m number of weeks (Table 4.1). The way the datasets were split into training and test sets is detailed in table 4.2. The train and test sets remained identical in all three model types.

TABLE 4.1: Available data and the number of extracted observations per site

Site	n_{house}	m_{week}	storage vessel observations	heat pump observations
A	8	96	2.93×10^5	4.53×10^3
F	4	32	5.50×10^4	7.83×10^2
R	53	32	6.20×10^5	2.42×10^4

TABLE 4.2: Training and test set size per site

Site	Training set ($n_{house} \times m_{week}$)	Test set ($n_{house} \times m_{week}$)	Train / test ratio (%/%)
A	8×64	8×32	67 / 33
F	4×16	4×16	50 / 50
R	32×32	21×32	60 / 40

4.1 Model performance

4.1.1 Storage vessel model performance

In this section the performance of the storage vessel model of Site R will be presented in detail (both black box and grey box). To easily compare the performance difference between the black box and grey box models, the results from both are always presented side by side. Results from the black box models are on the left, while the results from the grey box can always be found on the right.

Figure 4.1 shows the predicted water temperature distribution in the hot water vessel with increasing water consumption. The shaded area represents the 95 % prediction

interval of the ensemble. The initial temperature profile without any water consumption looks very similar in both of the cases. However the grey box prediction starts to differ considerably with increasing water consumption.

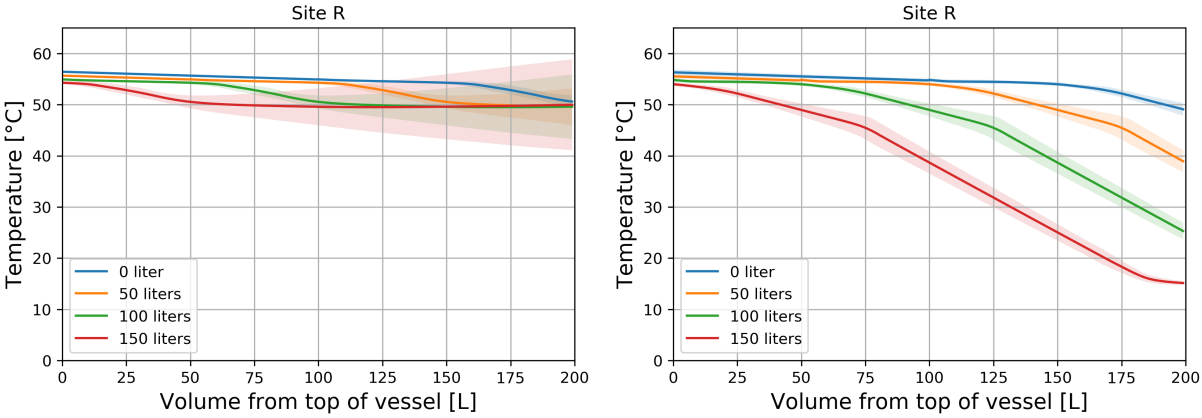

FIGURE 4.1: Predicted temperature distribution in the water tank with increasing water consumption
by black box models (left) and grey box models (right), given $T_{reheat} = 55\,°C$

Similar to figure 4.1, figure 4.2 presents the predicted temperature distribution and 95 % prediction intervals with increasing time passed since the start of the discharge cycle. Once again, the temperatures above the sensor are assumed to increase linearly with the volume. Although both black and grey box models predict decreasing water temperatures over time, they look quite different.

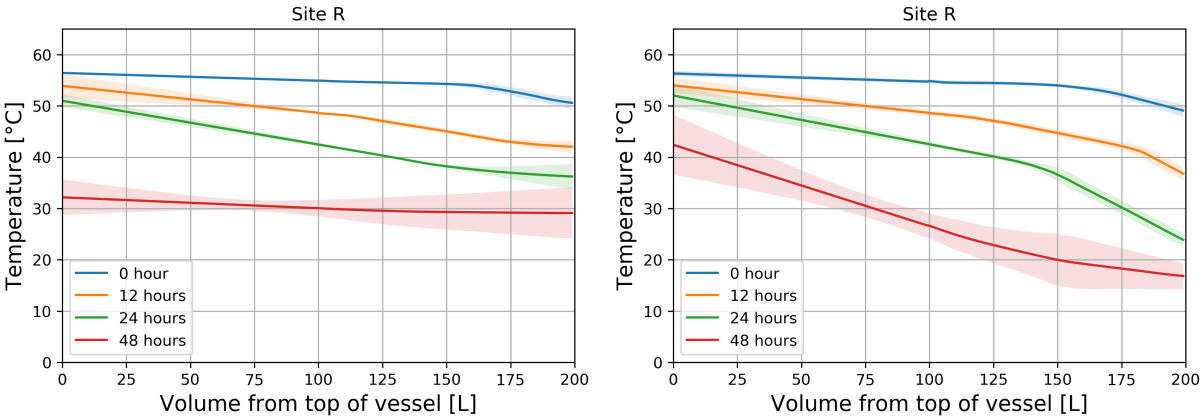

FIGURE 4.2: Temperature distribution in the water tank with increasing time since the start of the discharge cycle predicted with black box models (left) and grey box models (right), given $T_{reheat} = 55\,°C$

Although the temperature profiles (Fig. 4.1, 4.2) look unlike in the case of two model types, the mean absolute error is very close in both cases (Fig. 4.3). A MAE of around half a degree is comparable to the sensitivity of the temperature sensor (0.5 °C). The spread of

the prediction error shows a clear increasing trend with the decrease of temperature. This is expected as the lower the temperature, the more combination of input feature values belong to the same target temperature. On the top if that, the number of observations also decreases as the temperature decreases, which makes it more difficult for the model to learn the behaviour accurately. As seen in figure 4.4, the distribution of the error seems to be normally distributed, with a mean of about $\mu = 0°C$ and a standard deviation of $\sigma = 0.84°C$ in both of the cases.

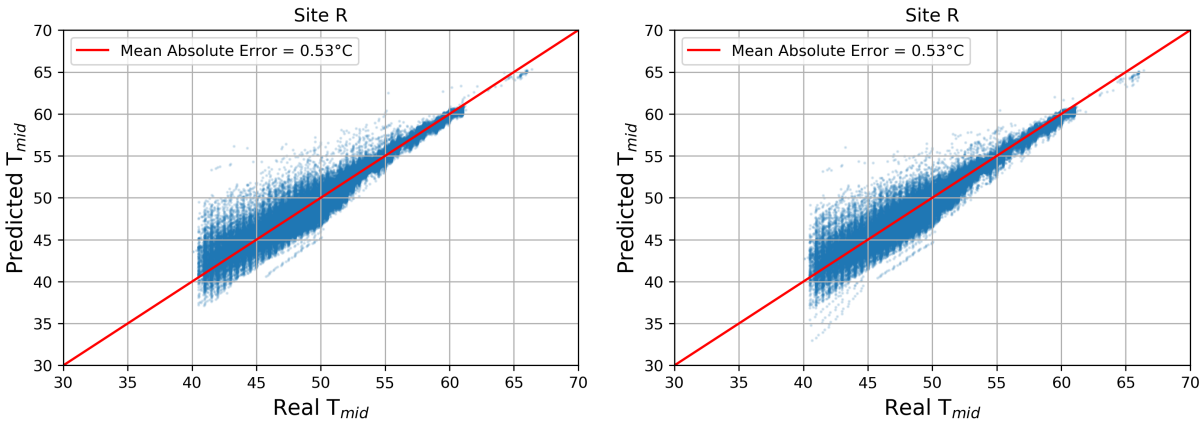

FIGURE 4.3: Mean of the predicted temperature with black box models (left) and grey box models (right)

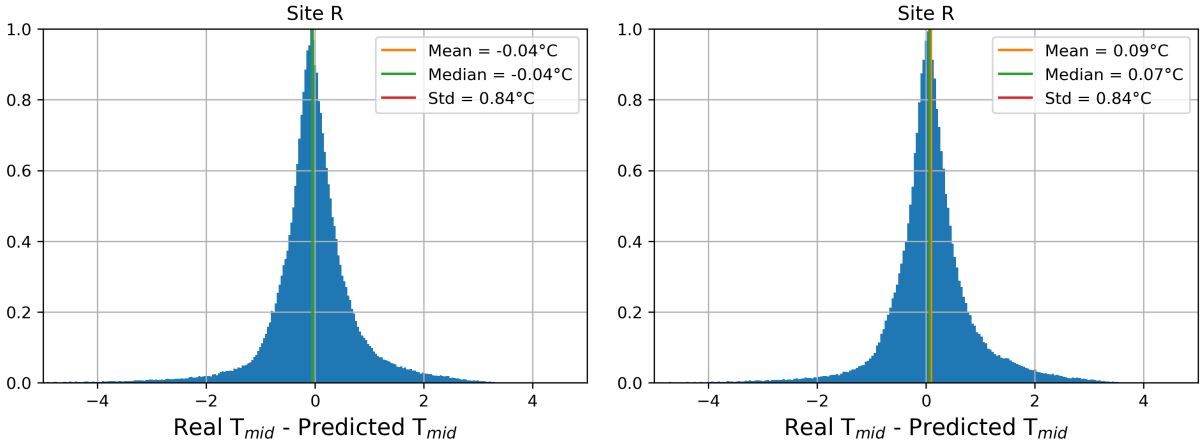

FIGURE 4.4: Distribution of the error of mean prediction with black box models (left) and grey box models (right)

After sorting the observations by the midpoint temperature for better understandability, figure 4.5 shows the real T_{mid} with 95 % prediction interval for all observation from the test set. As it can be seen, most of the time the midpoint temperature stays between 45 and 55 °C. The observations above 55 °C are due to the legionella cycle while below

45 °C are likely caused by a sudden drop in temperature due to high water consumption before the heat pump initiated the reheat cycle. There is a clear difference in the share of temperature measurements which falls into the prediction interval. Although 73 % of measurements fall in the prediction interval of the grey box ensemble, the prediction interval itself is also noticeably wider compared to the black box's.

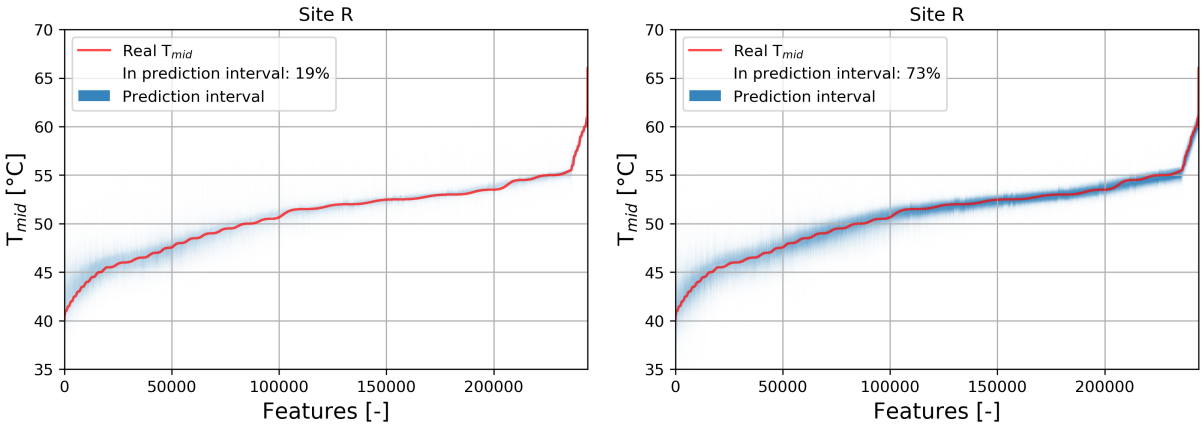

FIGURE 4.5: Sorted test observations by midpoint temperature, real target value (T_{mid}) and prediction interval with black box models (left) and grey box models (right)

Table 4.3 summarises the storage vessel model performances for all the sites. The black box and the grey box models gave very similarly results in all 3 cases. On the other hand, the models seem to perform better with increasing amount of data, as Site F had the least and Site R the most available data.

TABLE 4.3: Summary of storage vessel model performance per site

Site	Black Box MAE (°C)	Grey box MAE (°C)
A	0.64	0.65
F	0.98	0.92
R	0.53	0.53

4.1.2 Heat pump model performance

In this section the performance of the heat pump model of Site R will be presented in detail.

Figure 4.6 presents similarly to the storage vessel models the mean predictions of the heat pump ensemble on the left, and the spread of the prediction error on the right. The heat pump ensemble seems to learn to predict the energy well, with a MAE of 132Wh. This means between 5-30 % of relative approximation error in the majority of the cases. The standard deviation of the error shows a slight increase with the E, for similar reasons as in the storage vessel models (lower number of observation with increasing E and increasing number of input feature combination representing the same E). The spread of the heat

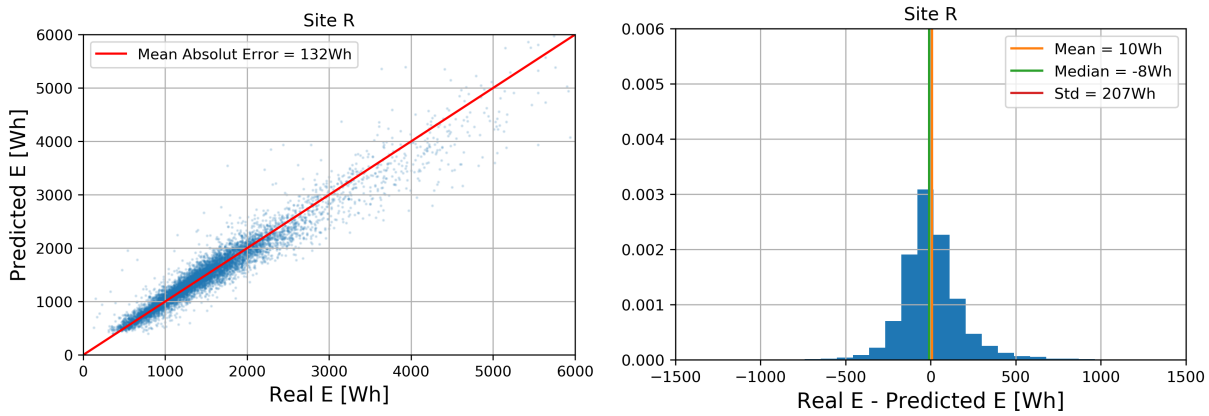

FIGURE 4.6: Mean predictions of the heat pump ensemble on the test set (left) and the spread of the prediction error (right)

pump prediction error also seems to fit a normal distribution with mean close to 0Wh and a standard deviation of around 200Wh.

The majority of the reheat cycles are consuming between 500 and 2000Wh (Fig. 4.7). As the data is collected through the autumn and winter with outside temperature below 0 °C for multiple days, some observations have higher consumption than 2000Wh. This can be explained with the variance in the HP's coefficient of performance with temperature. On the right hand side in figure 4.7 this trend is clearly captured by the trained models as the lower temperature always always corresponds to a higher E for the same reheat interval (T_{end} - T_{start}). As expected the E also increases with the increase of the reheat interval, even in the region where the model did not have any observations to learn from (T_{end} - $T_{start} > 15\,°C$).

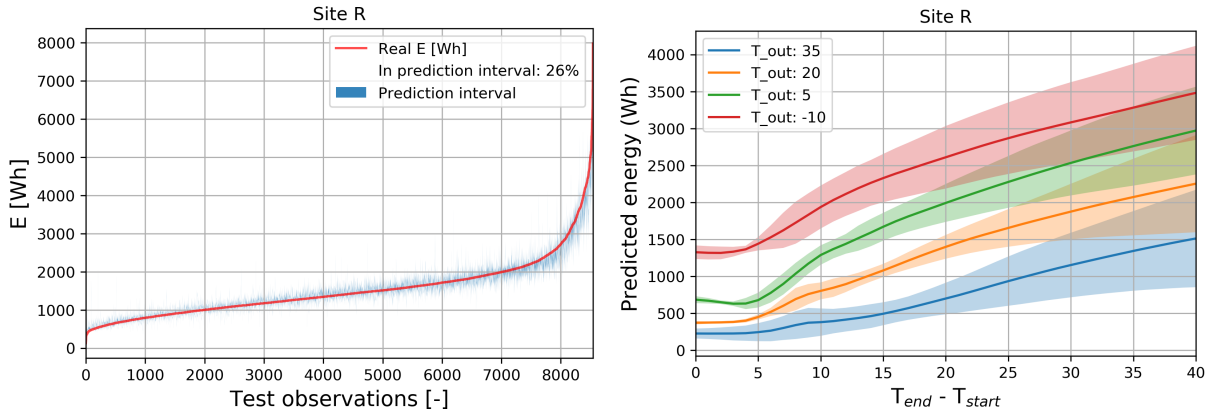

FIGURE 4.7: Sorted test observations by E consumption, real target value (E) in red and prediction interval of ensemble in blue (left), predicted E with prediction intervals for increasing reheat interval for different outside temperatures (right)

Table 4.4 summarises the heat pump model performances for all the sites. There is no noticeable performance difference between the 3 different sites.

TABLE 4.4: Summary of heat pump model performance per site

Site	MAE (Wh)
A	180
F	158
R	132

4.1.3 Model performance on other sites

The performance of the models from site A and site F are presented in this chapter. As the black box models are clearly underperforming compared to the grey box models in undiscovered areas of the state space, only the results of the grey box models will be presented. For easier comparison, the two sites will be presented side by side, site A on the left and site F on the right.

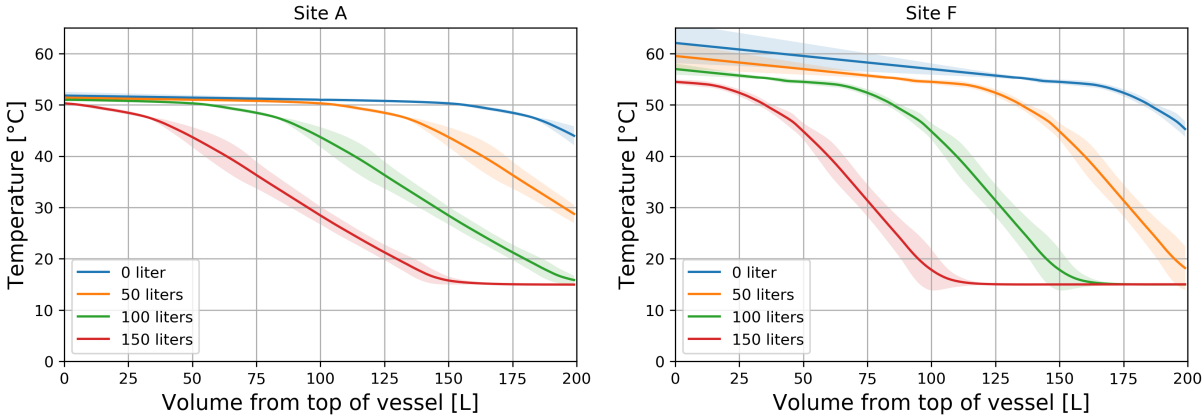

FIGURE 4.8: Predicted temperature distribution in the water tank with increasing water consumption given $T_{reheat} = 50\,°C$ for Site A (left) and $T_{reheat} = 55\,°C$ for Site F (right)

Figure 4.8 and 4.9 show very similar characteristics to the ones from site R. The results from site A are almost identical to the ones from site R, as site A has the same vessel on site, and had adequate training data. Even though site F had much less training data compared to the other two, the underlying characteristics look very similar.

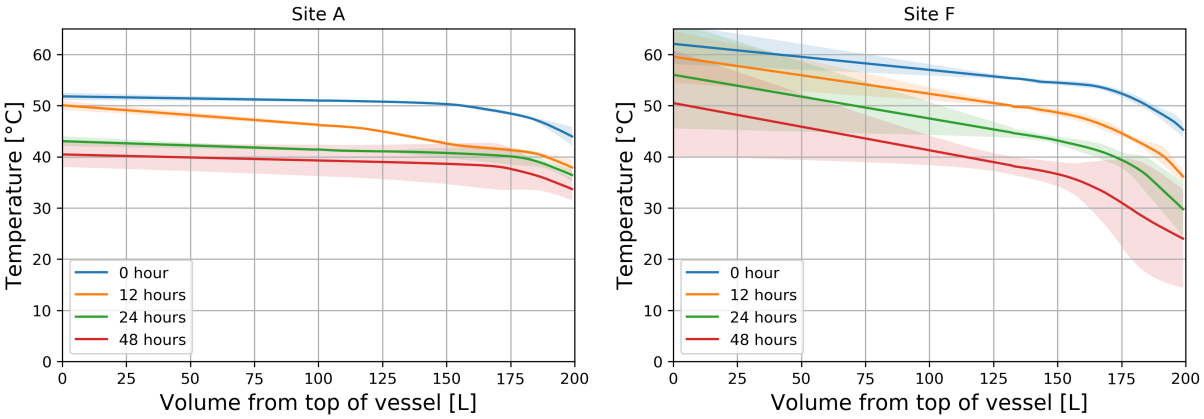

FIGURE 4.9: Temperature distribution in the water tank with increasing time since the start of the discharge cycle given $T_{reheat} = 50\,°C$ for Site A (left) and $T_{reheat} = 55\,°C$ for Site F (right)

Figure 4.10 and 4.11 present the prediction and the spread of the prediction error from sites A and F. The difference in operating zone is clearly visible from figure 4.10. The temperature of the vessel on site A drops as low as 40 °C, while on site F the vessel does not allowed to reach temperatures below 45 °C. Even though the models from these sites do not perform as well as on site R, this is mainly due to the lower amount of training data. This also seen in figure 4.11, where the error distribution of site F is not normally distributed.

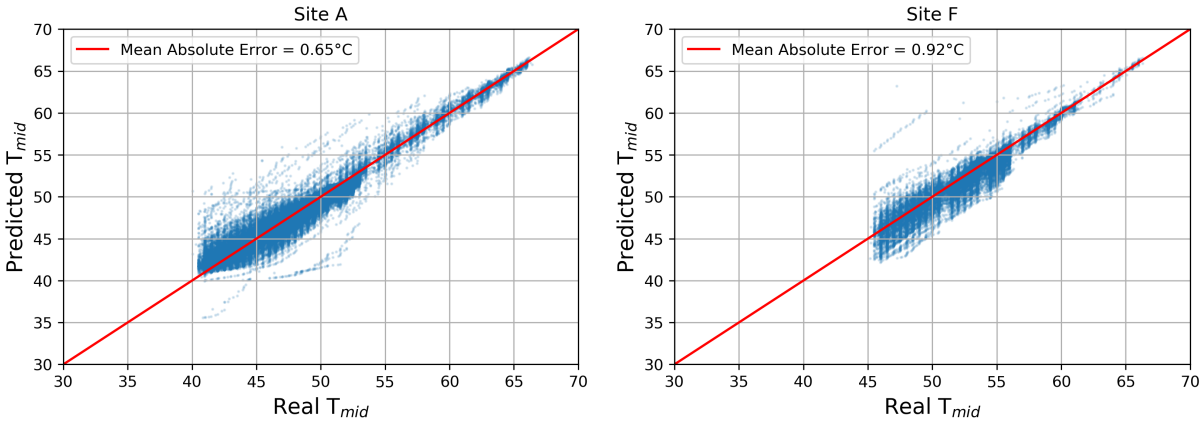

FIGURE 4.10: Mean of the predicted temperature with the storage vessel model of Site A (left) and Site F (right)

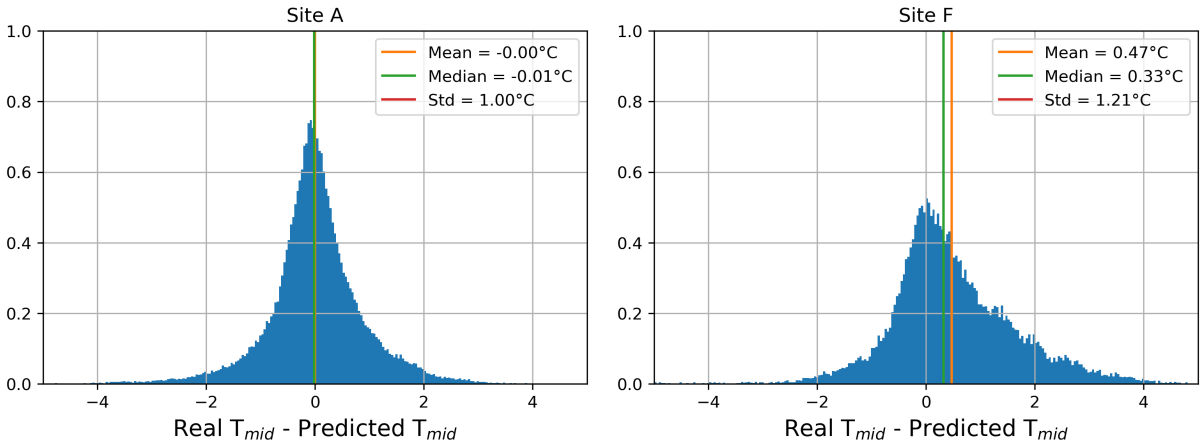

FIGURE 4.11: Distribution of the storage vessel model error of Site A (left) and Site F (right)

The difference in the operating temperature zone between the two sites is also shown is figure 4.12. Site A operates between 45 and 50 °C, while the vessels on site F are operated between 45 and 55 °C, where most of the observations are located. The increase in the prediction interval with lowering temperature is also present, as it was in the case of site R.

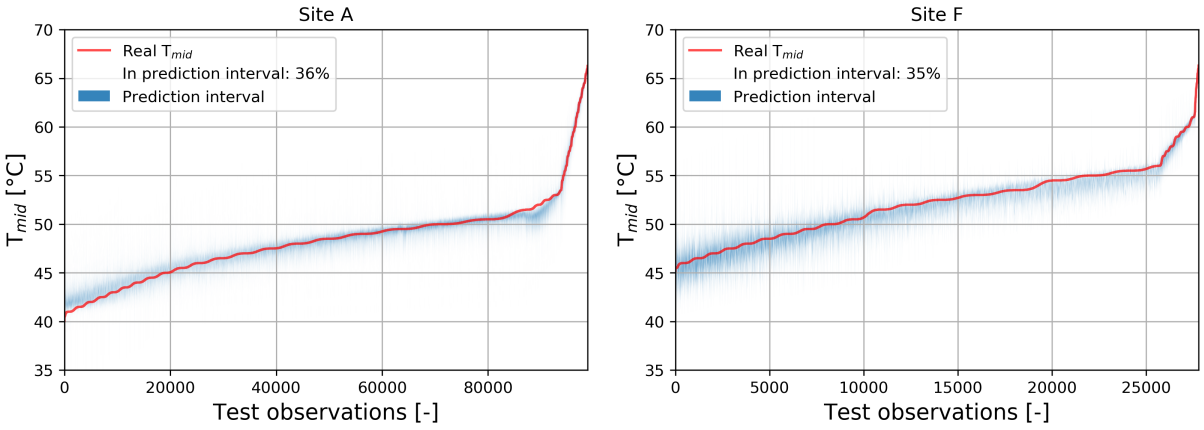

FIGURE 4.12: Sorted storage vessel test observations by midpoint temperature, real target value (T_{mid}) and prediction interval of site A (left) and site F (right)

The heat pump models from site A and F perform very similarly to the models from site R, as seen on figure 4.13 and 4.14. Unexpectedly, the heat pump models from site F achieved a lower mean absolute error than the models of site A, despite the lower number of observations. The models from site A and site F show normal error distribution with a mean close to 0, as in the case of site R.

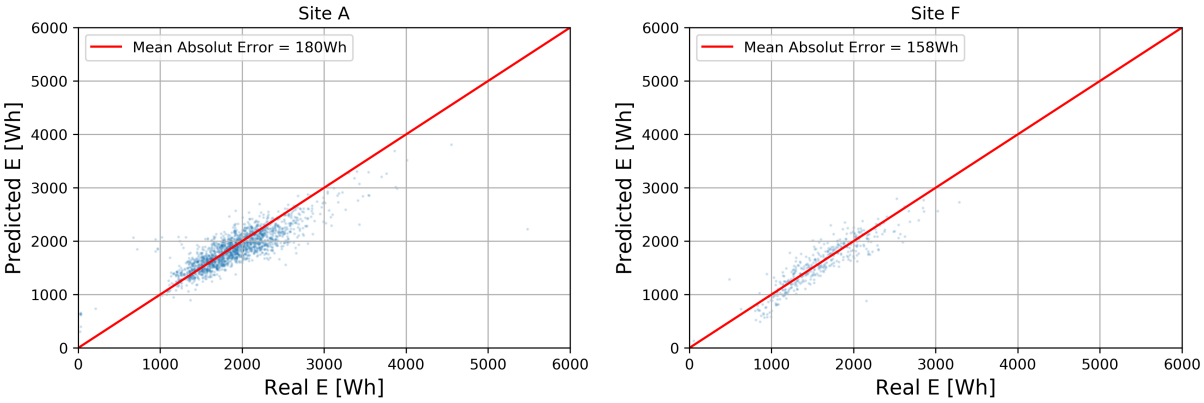

FIGURE 4.13: Mean of prediction of heat pump model ensemble of site A (left) and site F (right)

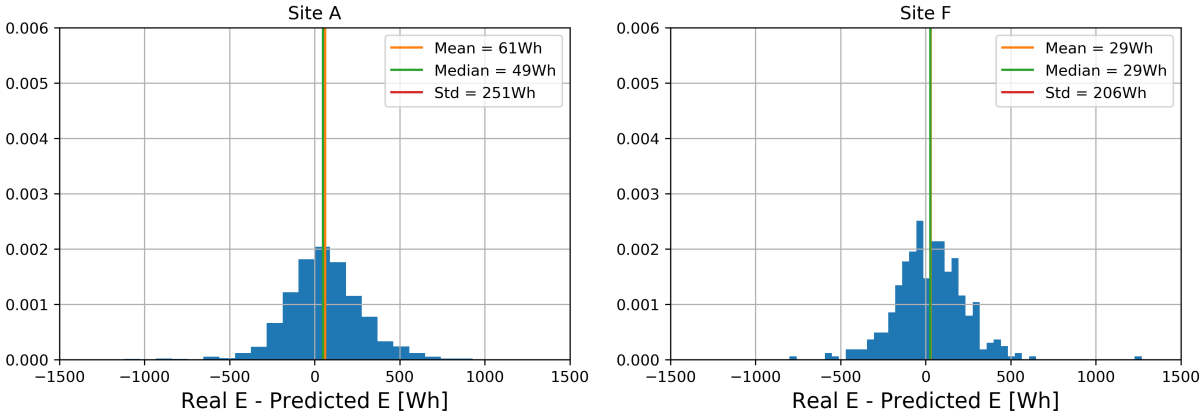

FIGURE 4.14: Distribution of the error of mean prediction of site A (left) and site F (right)

As seen on figure 4.16 both heat pump operates in a similar way as the heat pump on site R, taking between 500 and 3000 Wh to reheat the a 200L water tank.

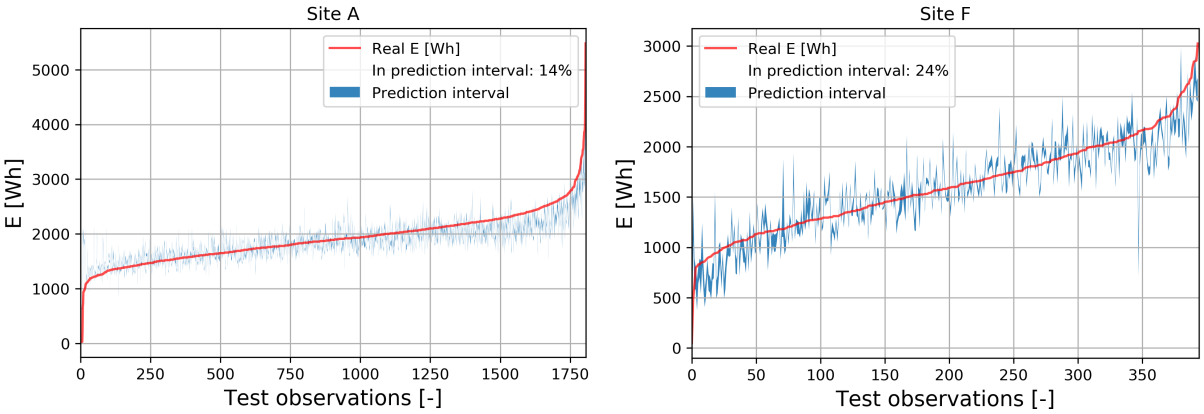

FIGURE 4.15: Sorted test observations by E consumption, real target value (E) in red and prediction interval of ensemble in blue for site A (left) and site F (right)

Despite the similar results in mean prediction error, figure 4.16 clearly presents the shortcoming of these model compared to the models of site R. These models were able to capture the trend between the ambient temperature and the energy demand, nevertheless they were unable to fully capture the trend between the temperature difference ($T_{end} - T_{start}$) and the energy demand. This caused by the lack of variety in control strategy. On site R, multiple different control strategies were implemented and tested during the data collection period, while on site A only the temperature set-points were changed for research purposes. On site F no alteration were executed, and the site F were controlled fully with the standard dead-band controller.

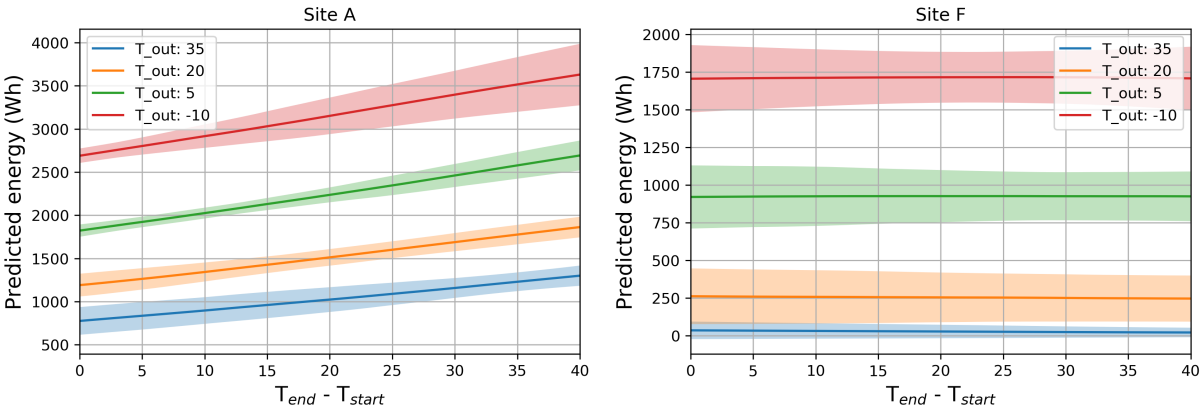

FIGURE 4.16: Predicted E with prediction intervals for increasing reheat interval for different outside temperatures (right)

4.2 Data influence

To investigate the influence of the amount of available data on model performance, the same steps introduced in figure 3.1 were performed on an increasing share of the dataset. Starting with data only from 1 house and during 1 week, the number of weeks is doubled until the total length of the dataset is reached (64 weeks in case of Site R). When reached, the number of houses is doubled and started again with only 1 week of data. This is repeated until the whole dataset is included. The amount of observations for each of these cases are shown in figure 4.17.

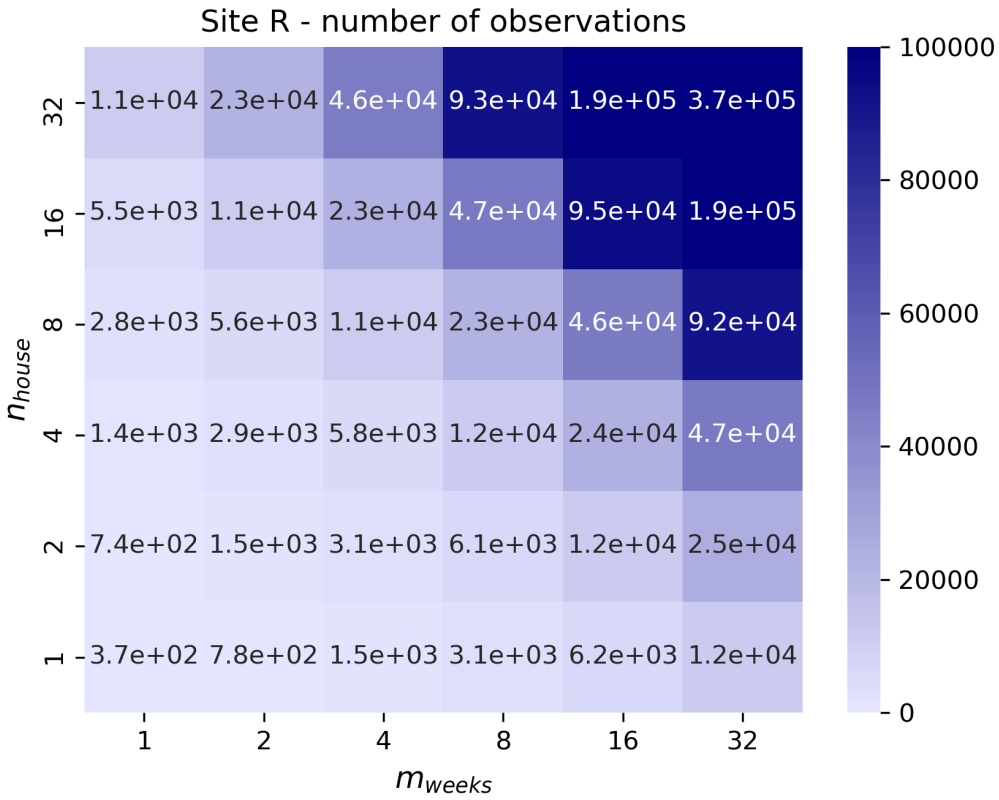

FIGURE 4.17: Number of storage vessel feature observations with increasing houses and weeks

Figure 4.22 shows the learning curve of the storage vessel and heat pump models over time for all the 3 different sites. Site A and Site R show very similar trajectory, Site R showing slightly faster error decay. As Site F still has not approached its asymptote, the fitted curve is not accurate enough yet to draw conclusions from it. The error decreases asymptotically and in the case of storage vessel models even approaching the temperature sensors sensitivity (0.5 °C). On the other hand, the effect on the one, sometimes two orders of magnitude difference in the number of observations between heat pump and storage vessel features is clearly visible. The storage vessel models take approximately 150-250 weeks (3-5 years) to reach its maximum performance, while the heat pump models require more than 20 years of data.

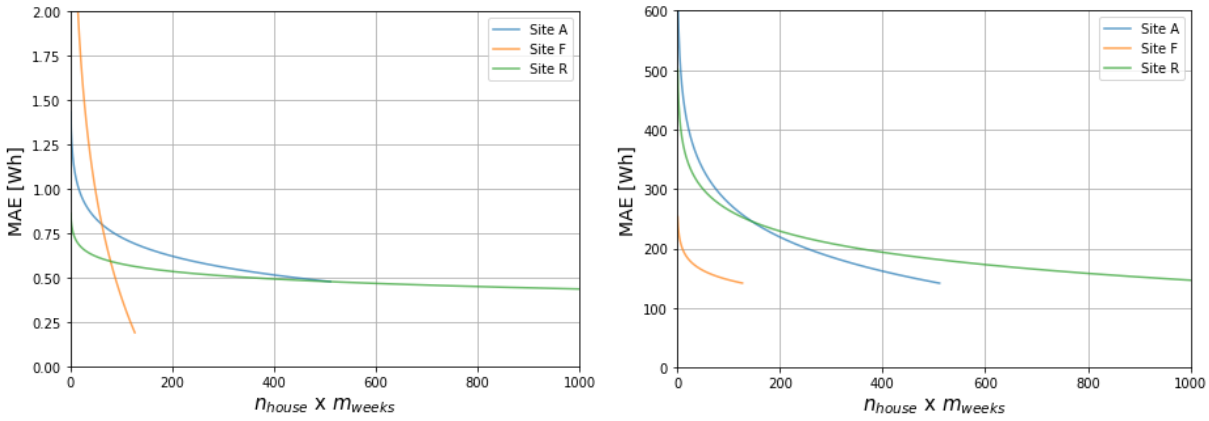

FIGURE 4.18: Mean absolute error of storage vessel models (left) and heat pump models (right) over time for all sites

4.3 Cross performance of models

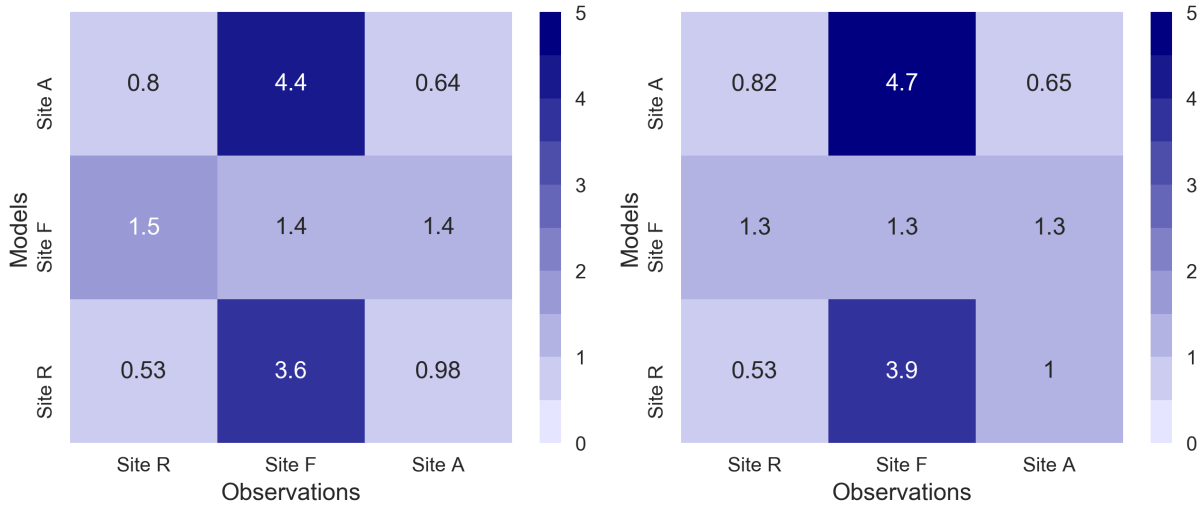

FIGURE 4.19: Mean absolute error of cross validated black box (left) and grey box (right) storage vessel models

To investigate the performance of these models on different, but similar kind of DHW storage tanks, the models from each site were cross validated on the observations from the others. The MAEs of the cross validated black box and grey box models are shown in figure 4.19 while the results with heat pump models are presented in figure 4.20.

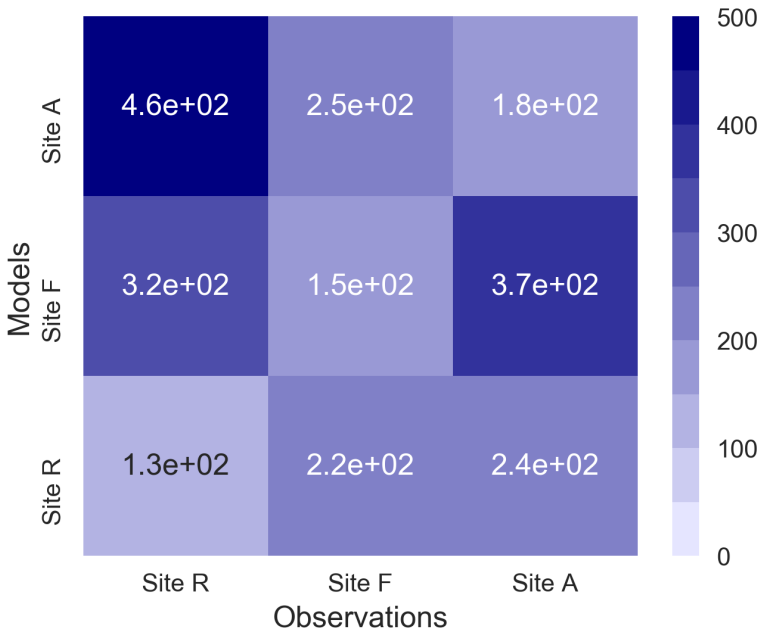

FIGURE 4.20: Mean absolute error of cross validated heat pump models

It is clear from the results, that the models always achieve the best results on the test observation from their own sites, while achieving varying results on observations from other sites.

4.4 Controller performance

The result of the simulations run with increasing threshold state of heat pump value for the energy efficient controller, later referred to as safety net is summarized in figure 4.21. As expected, a lower safety net (less hot water remained in the water tank when the reheat is initiated) is able to delay and lower the frequency of reheat which is resulting in less energy consumption. As the sensor in at the middle of the vessel in site R (and site A), the rule-based controller is equivalent to the energy-efficient one with 50% safety net resulting in 0% efficiency gain. Reducing the safety net to 25%, or 50L, a 10-20% efficiency gain is achieved in simulation, which is equivalent to the energy savings reached in real world tests. Eliminating the safety net could reduce the energy consumption by 20-35% albeit often violating the occupants comfort.

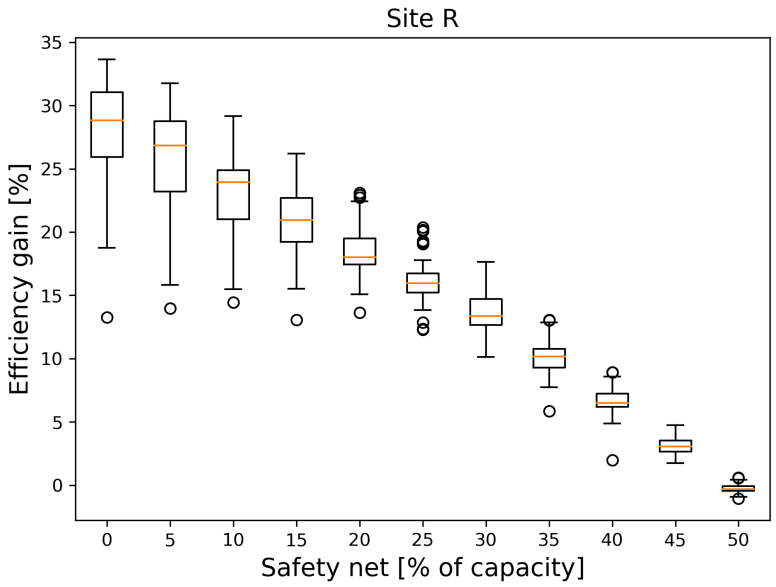

FIGURE 4.21: Efficiency gain by safety net size

When evaluating the performance of the energy efficient controller, two things needs to be taken into account: efficiency gain and occupant comfort. The controller performance in these two regards is presented in the left side of figure 4.22. On the right hand side the optimal safety net size by the chosen α parameter is shown. When α equals to 0, it corresponds to the maximalization of occupant comfort, therefore the maximum safety net size is the optimal. On the other extreme, when $\alpha = 1$ energy efficiency is prioritized over occupant comfort, therefore eliminating the safety net is optimal to maximize the energy savings.

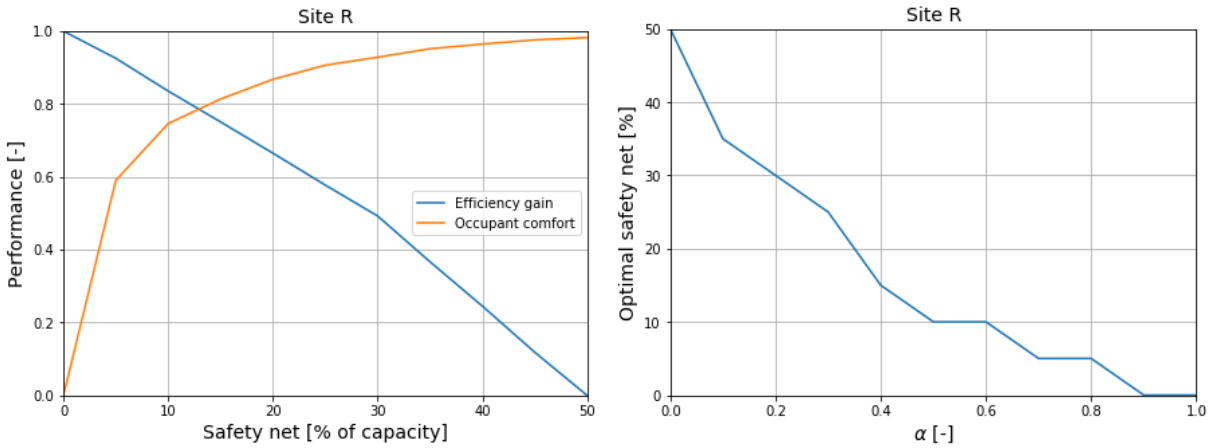

FIGURE 4.22: Normalized efficiency gain and occupant comfort with increasing safety net (left) and pareto frontier of the multi objective system (right)

4.5 Flexibility

4.5.1 Storage capacity - C_{adr}

Figure 4.23 and 4.24 show the storage capacity with vessels controlled with a rule-based controller (RBC) and an energy efficient controller (EEC) with 25 % safety net respectively. The results on the main graph were obtained by aggregating the 1 year simulation house-by-house and shown in Wh where a lighter color represents lower capacity and vice versa. The hour of the day is on the x axis, while the houses are sorted along the y axis by their daily average water consumption in liters.

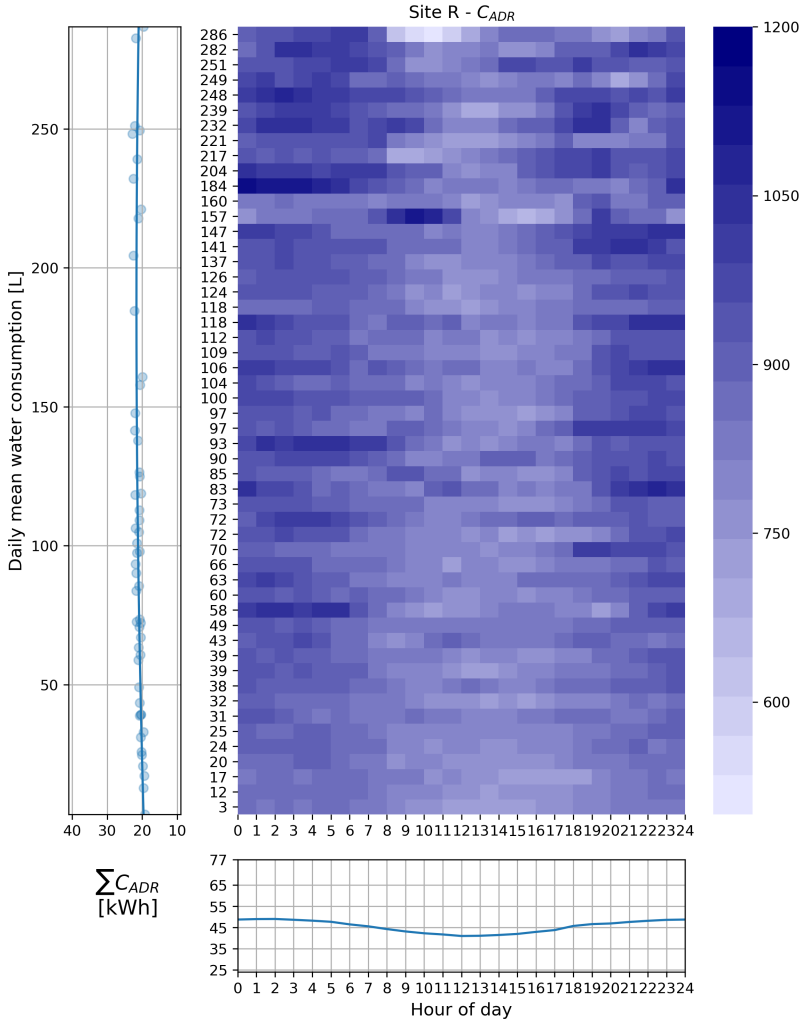

FIGURE 4.23: Hourly C_{adr} in Wh by household's daily mean water consumption aggregating a one year long simulation on a vessel controlled by rule-based controller, with plots of the hourly sum of C_{adr} for a site (bottom) and a daily sum of C_{adr} by the household's daily mean water consumption (left)

The hourly sum of storage capacity of all houses (y axis) is plotted under the main graph and represents the total storage capacity of a site during the day. The sum of capacity along the x axis (daily storage capacity of a house) is plotted on the left side of the main graph, and gives detailed information about the influence of occupant behaviour.

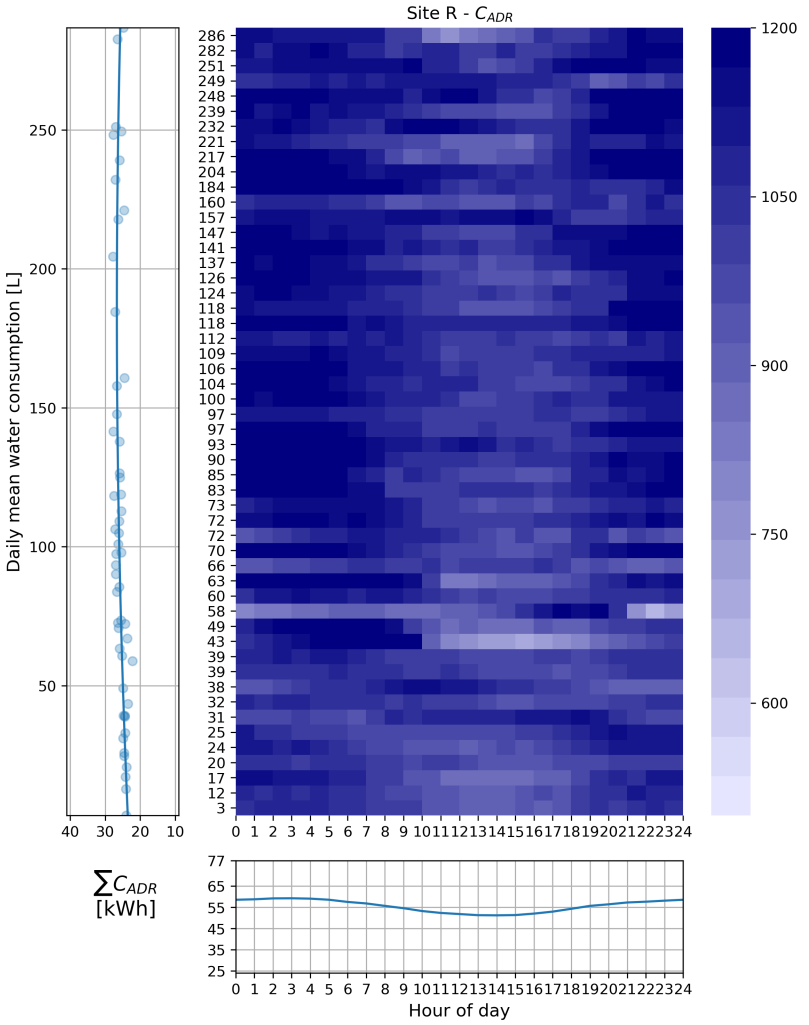

FIGURE 4.24: Hourly C_{adr} in Wh by household's daily mean water consumption aggregating a one year long simulation on a vessel controlled by energy efficient controller with 25 % safety net, with plots of the hourly sum of C_{adr} for a site (bottom) and a daily sum of C_{adr} by the household's daily mean water consumption (left)

Two similar trends can be observed on the two different controller. The ADR capacity is lower during the night and higher during the day. This trend is due to the ambient temperature difference, which has a high impact on the heat-pump's coefficient of performance. A reheat of the vessel with exactly the same state will therefore consume more energy if reheated during the night as if it happened during the day with higher outside temperatures. The second trend can be observed on the left graph in figure 4.23 and 4.24. The daily C_{adr} is the lowest with houses consuming very little water and increasing as the water consumption increases. The graphs suggest that this increase is not infinite, and the daily capacity reaches a maximum at around 200L of daily water consumption. As the water consumption level and patterns determine the state of charge level of the vessel, it also affect the ADR capacity. This suggest that households with at least average water consumption have slightly higher (10 %) positive flexibility potential.

When comparing the two controller methods, the energy efficient controller offers clearly higher flexibility in most of the household. While vessels controlled by RBC

generally offer between 700 and 1000 Wh storage capacity, EEC offers between 1 and 1.2 kWh. This corresponds to around 20 % higher site capacity at any given hour. A site with RBC offers between 40 and 50 kWh, while with EEC could offer between 50 to 60 kWh depending on the time of the day.

4.5.2 Storage efficiency - η_{adr}

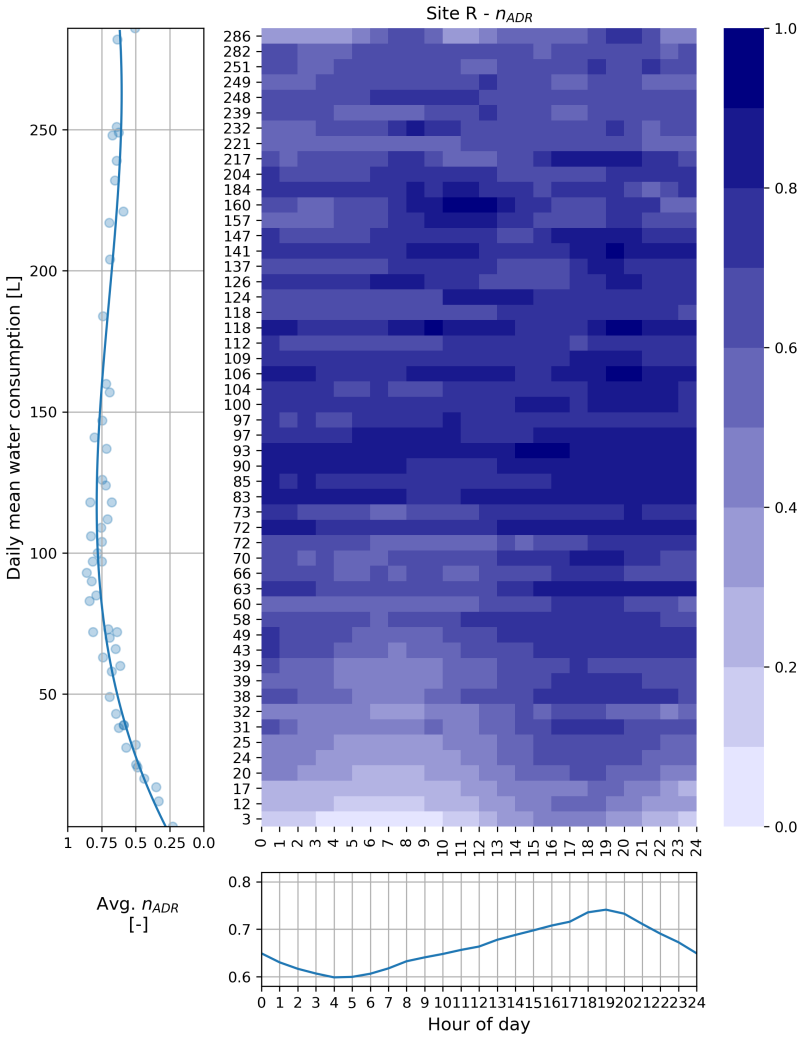

FIGURE 4.25: Hourly η_{adr} by household's daily mean water consumption aggregating a one year long simulation on a vessel controlled by rule-based controller, with plots of the hourly mean η_{adr} for a site (bottom) and a daily mean η_{adr} by the household's daily mean water consumption (left)

The storage efficiency is presented in figure 4.25 and 4.26, similarly to the C_{adr}. The hourly storage efficiency is presented along the x axis for a single household, sorted by the water consumption along the y axis. The average efficiency of the whole site along the day is shown below the main graph, representing the efficiency of an ADR event activated on the site at the given hour. The average efficiency of the households are plotted on the left side of the main graph, showing the effect of water consumption patterns on the storage efficiency.

The change in control strategy has a noticeable impact on the storage efficiency, especially in dwellings with very low water consumption. In these households, the η_{adr} reaches almost 100 % during every hour of the day, which represents a 30-70% increase compared to the rule-based controller. The houses with low to moderate water consumption levels were affected in the opposite manner, where the efficiency decreased from around 75 % to 55 %. The houses with high water consumption were the least affected with the control change and the storage efficiency stayed around 70 %.

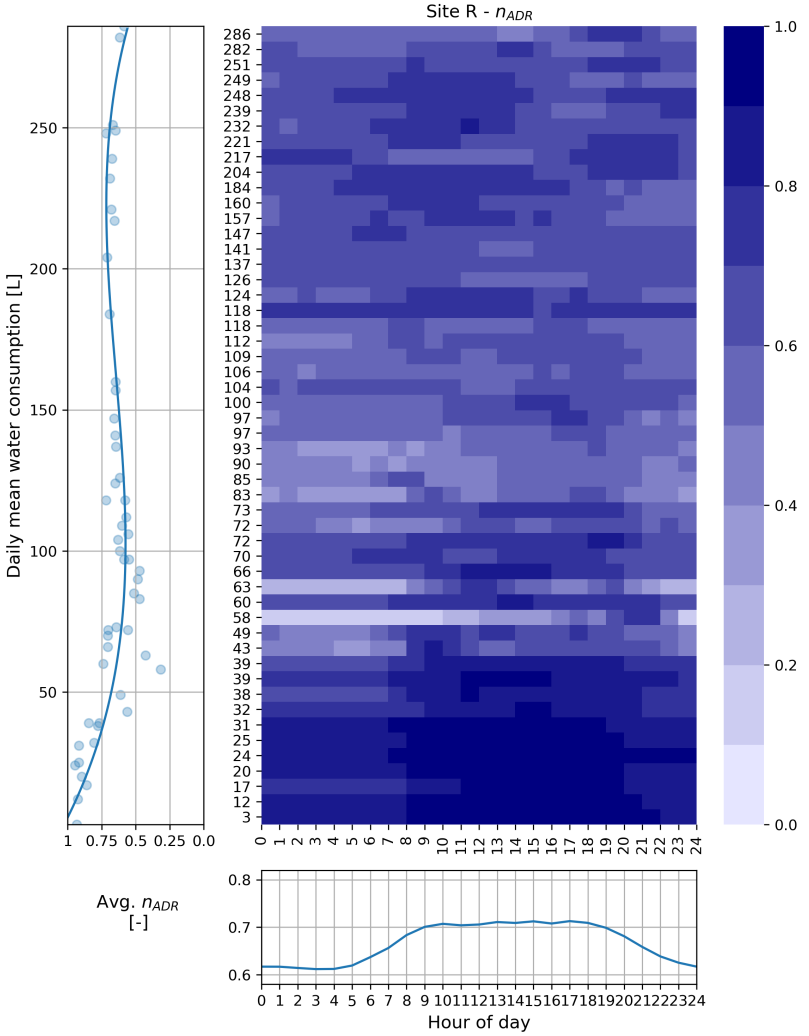

FIGURE 4.26: Hourly η_{adr} by household's daily mean water consumption aggregating a one year long simulation on a vessel controlled by energy efficient controller with 25 % safety net, with plots of the hourly mean η_{adr} for a site (bottom) and a daily mean η_{adr} by the household's daily mean water consumption (left)

During the day there is only a few percent efficiency difference between the two control methods. The average efficiency is higher during the evening (between 16 o'clock and 4 o'clock in the morning) with the rule-based controller, while the energy efficient control stores the energy more efficiently between 5 o'clock in the morning and 16 o'clock.
Generally, the efficiency of an ADR event falls between 60 and 70 %, being lower from late night until early morning and higher during the day. Household with water consumptions

below 50L are the only exception, where the efficiency is highly dependent on the control strategy. Here the efficiency can range from 25 to almost 95 %.

4.5.3 Power shifting capability - Q_d

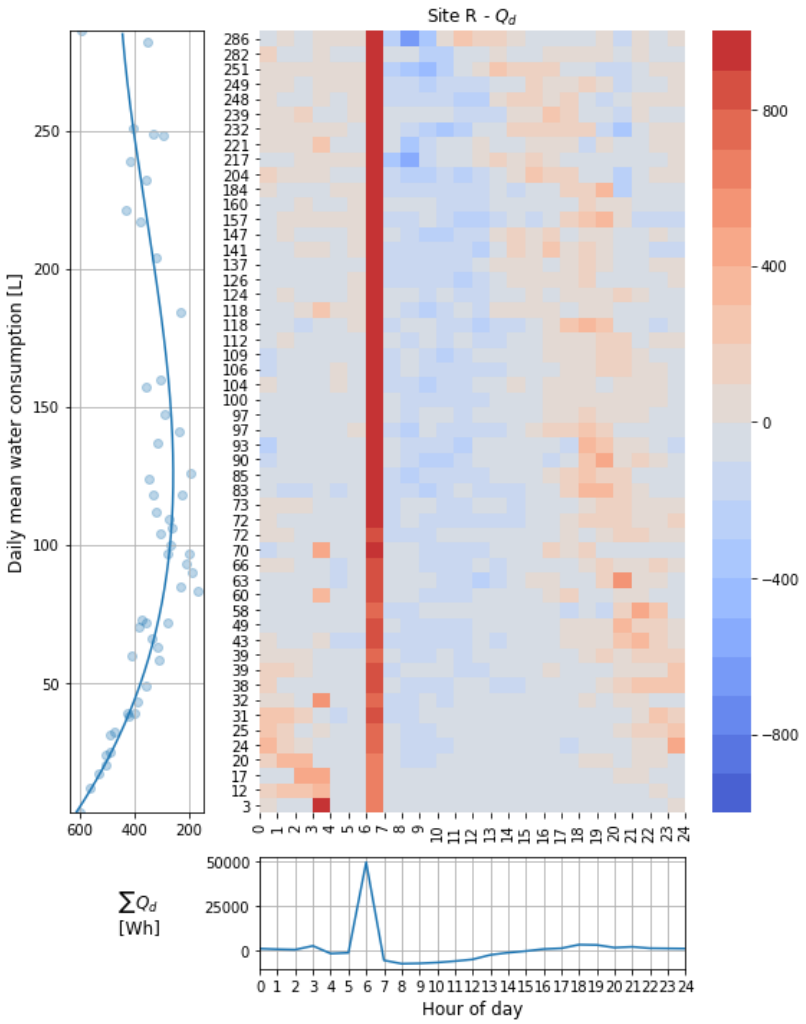

FIGURE 4.27: Power shifting capability Q_d by household's daily mean water consumption aggregating a one year long simulation on a vessel controlled by rule-based controller, with plots of the hourly mean Q_d for a site (bottom) and a daily mean Q_d by the household's daily mean water consumption (left)

Figure 4.27 and 4.28 shows the Q_d over the day with rule based controller and energy efficient controller respectively, with an ADR activation hour of 6 o'clock. This time of activation is clearly visible as a red vertical line, when the ADR activation increases the energy consumption significantly compared to the original behaviour. A rebound effect is present after the activation, where the Q_d turns negative for some period. This period is longer in houses with low consumption and gets shorter as water consumption increases as anticipated. After the negative period a second positive peak can be observed, albeit generally much lower than the peak at activation. An exception can be found with extreme

low water consumption using the rule-based controller. Here a clear second peak is visible 22 hours after activation.

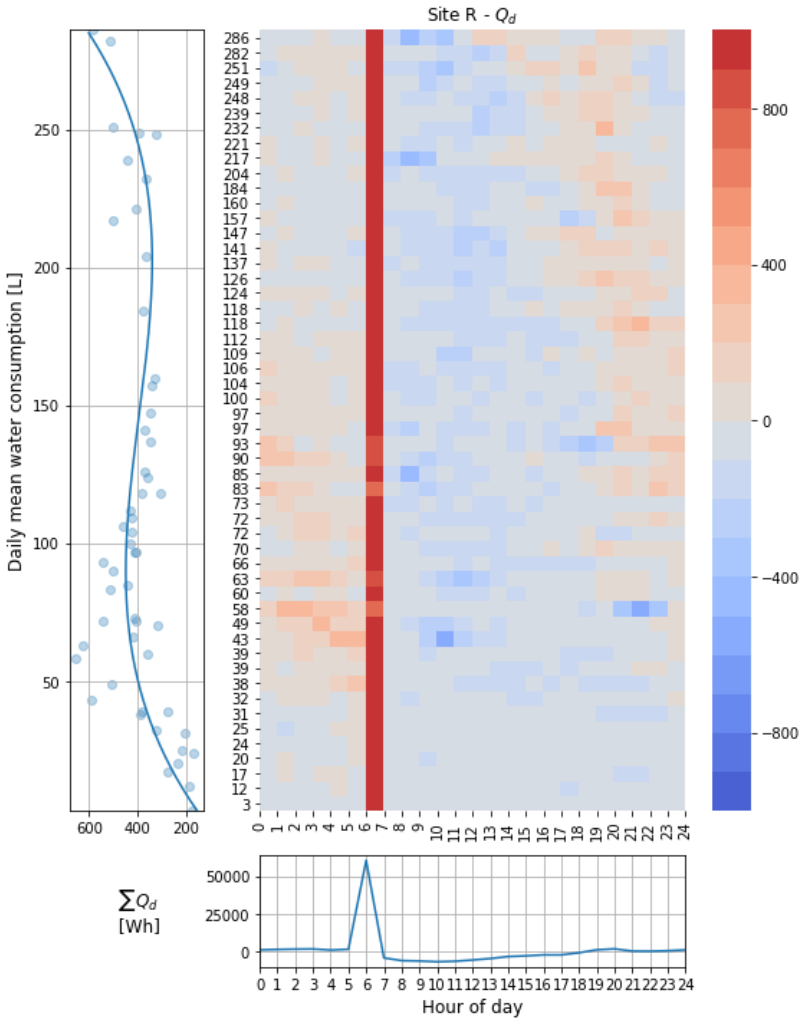

FIGURE 4.28: Power shifting capability Q_d by household's daily mean water consumption aggregating a one year long simulation on a vessel controlled by energy efficient controller with 25 % safety net, with plots of the hourly mean Q_d for a site (bottom) and a daily mean Q_d by the household's daily mean water consumption (left)

Compared to the rule-based controller, a generally longer recovery period can be observed due to the energy efficient controller (Fig. 4.28). In household with very low water consumption (lower that 30L per day) the recovery period is higher than 24 hours, which results in a lower storage capacity as seen in figure 4.24. The difference in recovery period between the two controller is shown in figure 4.29 averaged for all houses on site. The general trend is clear that the energy efficient controller lengthen the recovery period with 2-3 hours in average compared to the rule-based controller, just as it increases the average time between reheat cycles.

The graph on the left side in figure 4.27 and 4.28 shows the sum of Q_d through the day for each houses. These graphs follow the trend of the efficiency curves in reverse as the daily sum represent the energy loss due to the demand response event.

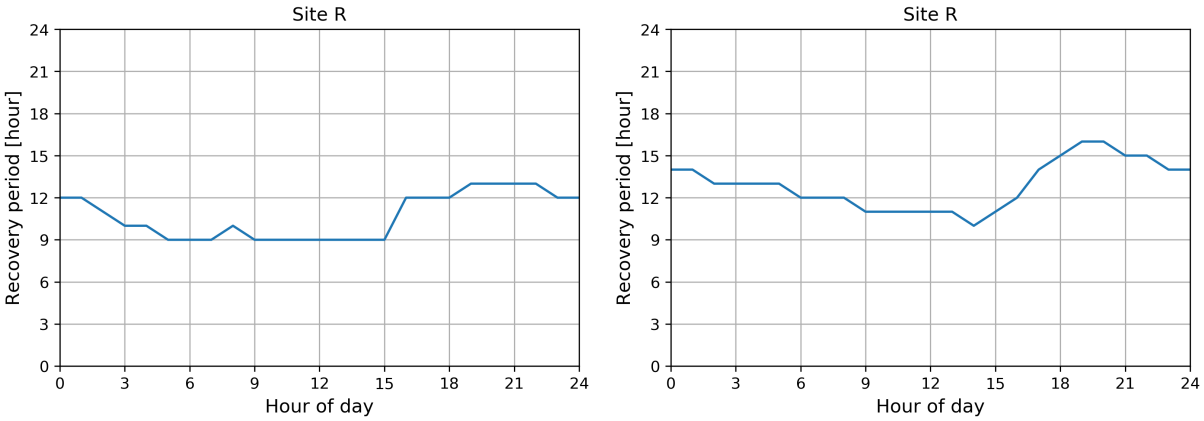

FIGURE 4.29: Average site recovery period by different activation time during the day with rule based controller (left) and energy efficient controller (right)

4.5.4 Seasonality

As seen earlier, the ambient temperature has a strong influence on the potential flexibility and its efficiency. The seasonal trend in the above detailed parameters are presented in figures 4.30 - 4.32.

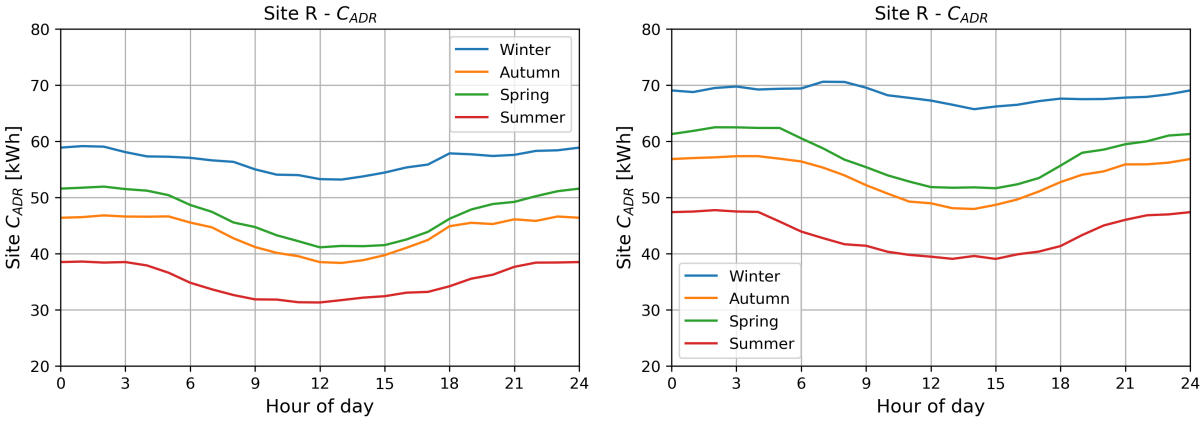

FIGURE 4.30: Seasonal site storage capacity during the day with rule based controller (left) and energy efficient controller (right)

As expected, from the daily trend in the storage capacity, a lower ambient temperature increases the available capacity due to the lower heat pump efficiency. This results in around 50 % higher capacity during winter than summer (fig. 4.30). The flexibility during spring and autumn are around halfway between the capacity during winter and summer. The energy efficient controller offers around 15 % higher C_{ADR} than the rule-based controller, as shown before.

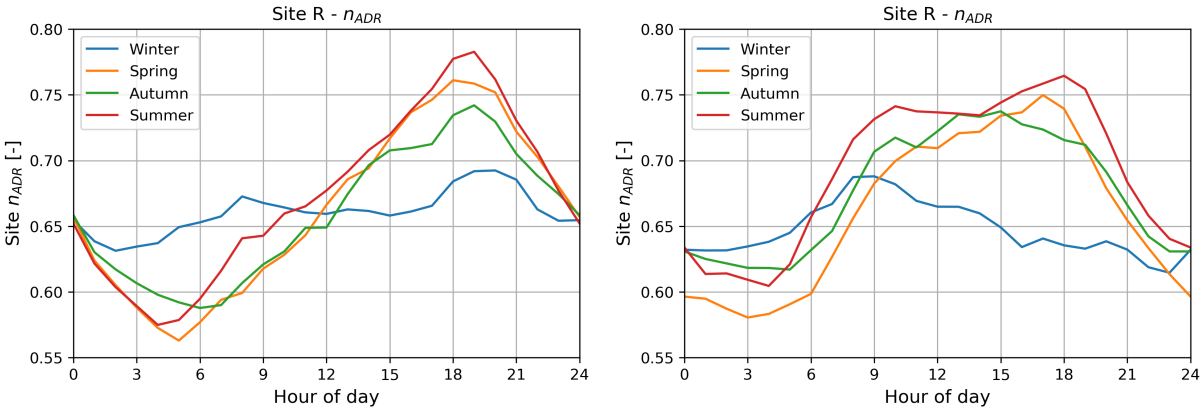

FIGURE 4.31: Seasonal site storage efficiency during the day with rule based controller (left) and energy efficient controller (right)

The storage efficiency on the other hand shows a different seasonal trend (fig. 4.31). The η_{adr} during the day follows the same trajectory from spring until autumn, while have a much flatter one during the winter with both controllers. The lower ambient temperature clearly has a positive effect on the storage capacity, while decreasing the storage efficiency, Both are direct consequence of the usage of a heat pump.
The recovery period does not show any influence from ambient temperature and has very similar daily profile during the whole year (fig. 4.32). This would imply that there is no seasonal trend in water consumption, but this cannot be ruled out as the used water consumption profile in the simulation was randomly chosen. It is reasonable to assume that the season affects the hot water consumption profile, as people tend to take hotter shower during the winter and colder during hot summer periods.

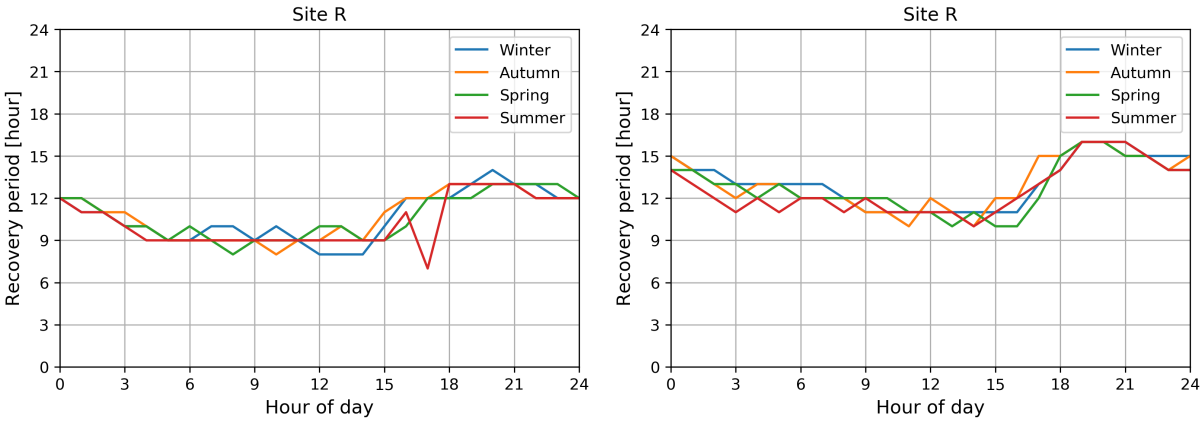

FIGURE 4.32: Seasonal recovery period of the site during the day with rule based controller (left) and energy efficient controller (right)

Chapter 5

Discussion

5.1 Model performance

Based on the previously detailed results, it can be said that the neural network performed very well on all types of models without changing its architecture. In the case of storage vessel models the NN's accuracy even approached the resolution of the temperature sensor installed in the vessel (0.5 °C), which acts as a limit on the achievable accuracy. The heat pump models also achieve remarkable accuracy, given that they have not reached their maximum performance yet. A mean absolute error of around 150Wh corresponds to 5-15% accuracy, with a potential to reduce it to below 100Wh.

Having said that, it must be mentioned that these models were only tested in a small region of the state space. These vessels were only controlled with tight comfort constrains, therefore the diversity of the data is rather limited. This is clearly visible in figure 4.3, where the uncertainty of the prediction increases with decreasing midpoint temperature. First of all, during normal operation an increasing part of the state space correspond to the same T_{mid} as the temperature decreases, as there are more and more ways to reach that lower temperature (e.g. with quick and fast water withdrawal or by letting the tank loose that energy over a long time period without water consumption). Secondly, the amount of available data also decreases as the midpoint temperature decreases. This is understandable as the controller tries to keep the midpoint temperature between the set temperature boundaries, and the only way to experience the part of the state space with lower T_{mid}s, is with sudden, high amounts of water consumption close to the lower temperature boundary.

Based on the above mentioned factors the conclusion can be made, that the introduced neural network model is capable of modelling the behaviour of both the hot water tank and the heat pump with high accuracy only with small adjustments to the hyperparameters. However, its performance is limited by the data collecting sensors' resolution and high accuracy is limited to the part of the state space where training data is available.

5.1.1 Black or white?

As seen in chapter 4.1.1 both black box and grey box models performed very similarly with a difference in MAE of only a few hundreds of °C. Still, their predicted water temperature profiles look increasingly different as the tank gets discharged (Fig. 4.1, 4.2). A fully charged water tank temperature profile looks very similar when predicted by either of the two models. However when comparing the profiles with high water consumption, or a long time after the reheat, the grey-box model predict a much steeper temperature profile along the height of the vessel. Intuitively, the black-box model clearly underperforms

outside of the encountered state space as it predicts temperatures above 50 °C along the entire height of the vessel, even with water consumptions higher that the capacity of the vessel. As the incoming water's temperature is around 10-20 °C (depending on the season) which replaces the hot water inside the vessel, it is easy to understand why this is far from reality. The grey-box model on the other hand was able to capture the trend caused by the cold water inflow.

Even though the grey-box model seems to model the vessel more realistically, this performance difference is not reflected in the numbers, as the models are not tested in these states. The lowest T_{mid} encountered in the test set is around 40 °C, therefore it is impossible to confirm which model is performing better outside of the tested state space. Based on domain knowledge, it is reasonable to assume, that the pure data driven black-box model would be increasingly similar to the grey-box model, if the training data is covering a bigger part of the state space. In case the full state space is covered, it can be assumed that the black-box model error would be lower compared to the grey-box one, as the added domain knowledge is an oversimplification of the real system.

5.1.2 Agent or agency?

As discussed above, the quality and quantity of the data has a high influence on the models performance. Therefore the amount of required data is an important parameter of the model. Figure 4.22 summarized the models' performance by increasing data amount. As expected, the accuracy of the models is decreasing super-linearly with the increase of training data. This effect is also apparent when comparing the 'learning rate' of the storage vessel and heat pump models. The storage vessel model collects around 50 observations during one day per house, while the heat pump model only collects 2 observations per day in average. This allows the storage vessel model to decrease its error much quicker.

The multi agent systems perform on par with the single agent ones when comparing them with the same amount of data. This confirms that training time of a single agent is interchangeable for another agent with similar properties. Due to this a learning task that would take 1000 weeks (20 years) for a single agent, only takes a weeks for an agency with 1000 agents.
In some cases the multi agent system outperformed the singe-agent ones with the same amount of data. This can be explained with the increase in the explored state space with a growing agency as every agent has a slightly different behaviour. This difference in the size of the explored state space is shown in figure 5.1, comparing a single agent with an agency of 32 agents.

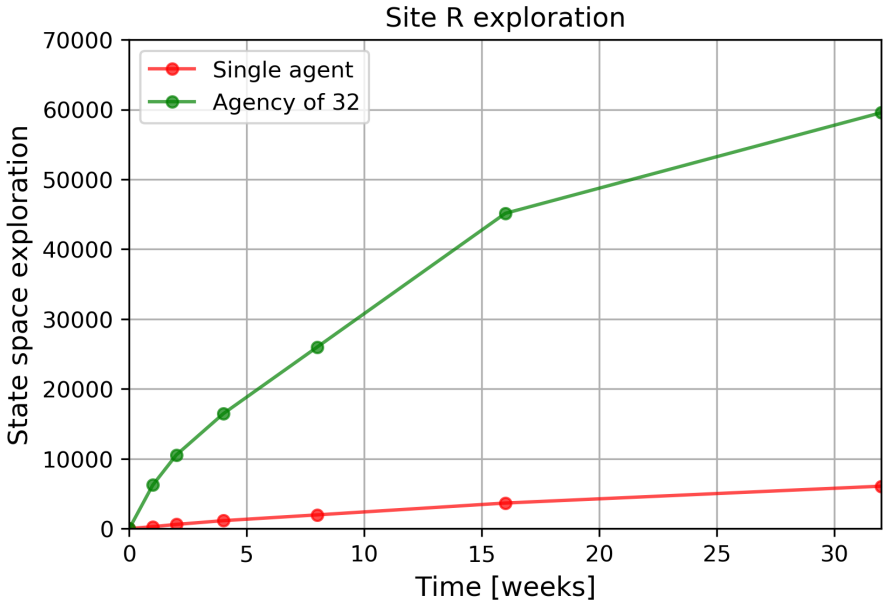

FIGURE 5.1: Size of the explored state space by time with a single agent and an agency with 32 agent

5.1.3 Do we get free lunch?

When combining the results from all three sites, and the results from both storage vessel and heat pump models, it can be said with confidence, that the same neural network model structure was able to capture the underlying nonlinear mechanics of both systems, making it generalizable to some extent.
As seen in figure 4.19, when comparing models from a site performing on other sites with similar physical equipment, the models perform reasonably well. All 3 sites had a storage with 200L capacity, with a single sensor at the midpoint on site A and R, while site F had the sensor at 1/3 of its height. Site A and Site R use the same type of vessel, only using different control strategies and operating in different temperature boundaries, which explains the slight increase in the error when predicting on each others observations. As Site F uses a different storage tank, the other models fail to predict it's behaviour accurately, with a MAE of 3-4 °C. This limits the generalizability of the storage vessel model to only similar water tanks. It is also not very practical to used a model trained on another vessel, as a model of that vessel would perform better in just a few months.

Similarly, the generalizability of the heat pump models are limited to identical heat pumps. All sites have different heat pump units, which is reflected in the cross site performance of these models. However the benefits are significant when using a model from another site, as these models take much longer to reach their maximum performance (Fig. 4.20). Using a model trained on a dataset form another type of heat pump could provide an instant performance level which would take more than 100 weeks of data to achieve.

5.2 Control methods

Using simulations, energy efficient controller were able to achieve up to 30% energy savings on site A and R and 65% on site F compared to the standard rule-based controller. These saving under real life conditions would not be possible, as eliminating the safety net would result in a disfunctioning hot water vessel. However with only 10% in of loss in occupant comfort, almost 60% of the maximum achievable energy saving is reached, which correspond to an $\alpha = 0.3$. In some lower standard dwellings this could be further increased to 0.4, thus capturing 80% of the saving potential with 20% occupant comfort loss. Further increasing the α parameter would have diminishing returns at an increasingly higher loss in occupant comfort.

All this saving potential is achievable without increasing the computational and operational complexity of the controller. In case the model is preloaded onto the vessel, even ICT technology would not be necessary, albeit losing the potential for further learning and improvement. Either with or without ICT, the control can be executed locally without additional computational power.

5.3 Simulation results and flexibility indicators

All simulation results were obtained using the grey-box models, as they were proven to be more robust in regions outside of the training set and let a wider range of states to be simulated.

Based on the results, the following factors influence the flexibility in these buildings:

- ambient temperature
- control strategy
- occupant behaviour

The first two seem to have the highest impact on storage capacity, while occupant behaviour has only minimal impact on the C_{ADR}. The low ambient temperature increases the storage capacity, because these vessels are using a heat pump as a reheat unit. Therefore the effect of ambient temperature is case specific and will differ in DHW tanks with different reheat units. The energy efficient control algorithm is able to increases the storage capacity, with the reduction of the safety net and lower average SOC levels. Occupant behaviour had the lowest impact on storage capacity compared with the other two. The capacity of tanks in houses with low water consumption profiles (<50L/day) are lower than rest of the houses, likely due to the long recovery period, lowering the average storage capacity in a daily activated setting.

The change in control algorithm also has significant impact on the storage efficiency, especially in dwellings with low water consumption. As seen in figure 4.27, the water tank reaches the RBC's threshold temperature in less than one day (around 22 hours with negligible consumption). This means that a daily active demand response would add an additional reheat cycle where only 1 happens in average, thus increasing the total consumption and lowering efficiency. As the energy efficient controller is able to postpone the reheat by allowing lower SOC levels, the active demand response only shifts the time of reheat without adding an additional one, increasing the efficiency from around 25% up

to around 95%.
Occupant behaviour and patterns has a much higher impact on the storage efficiency compared to the capacity. In some houses with strong regular patters this effect is highly visible in figure 4.26 reducing the efficiency close to 0% during most of the day, and having almost 100% for short periods. In general, the efficiency follows the daily consumption profiles, increasing the average site efficiency during the day to 70% and lowering it down to 60% during the night. This behaviour is expected, as the heat added by the ADR event during the day would be utilized by hot water consumption compared to an ADR event in the late hours, where most of the added heat would be lost in thermodynamic losses.

As expected, the consumption habits of the occupants also has an impact on the power shifting capability and recovery period. A storage tank is able to recover the faster after an ADR even in households the higher the consumption. Low consumption levels and the decrease in safety net both increase the recovery period, in some cases even above 24 hours, reducing the storage capacity potential in case of a daily scheduled ADR event.

The seasonal trends in these parameters are expected based on the influence of ambient temperature. The same household in a colder climate or season could offer higher storage capacity less efficiently. It is expected that seasonal consumption patters will further influence these parameters, but this was not investigated due to the insufficient data amount.

As seen in figure 4.27 and 4.28, an ADR event can have significant impact on the load profile of a house, let alone on the distribution grid. During normal operation, the reheat events of the tanks spread out evenly during the day, flattening the aggregated load profile. A collective and simultaneous ADR event on a site would create a not insignificant peak in the load, which could cause voltage dips or even overload a distribution grid. With intelligent control however, the flexibility of the water tanks could be used to provide various services detailed in chapter 5.4.

5.4 Potential business applications

Increasing efficiency of heat pump units and rising shares of electricity provided by RES make HPs an increasingly attractive and ecologically favourable heating solution. As demonstrated, these paired with a storage unit are able to provide flexibility. Utilizing this flexibility with advanced control and communication technologies, the HP operator could provide various services to third parties. However, flexibility will only be used if economically attractive and technologically feasible business cases can be identified. Fischer et at. performed a detailed techno-economical analysis of different business models using a single family house equipped with a 5 kW_P PV plant in Germany [67]. The results of this analysis is presented in table 5.1, broken down into technical, costs, revenue, risk & complexity and attractiveness sections.

The following business models were analysed:

1. optimised electricity purchase at the spot market
2. reducing balancing power need
3. primary reserve
4. secondary reserve (both positive and negative)

5. tertiary reserve (both positive and negative)
6. reduce grid fees (by allowing load interruption or load shifting to low tariff periods)
7. increased PV self-consumption
8. improved energy efficiency (by utilizing weather forecast, operational data and sophisticated control algorithms)

TABLE 5.1: Attractiveness of the investigated business models divided into technical, costs, revenue and risk aspects [67]

	Purchase	Grid services and balance group management							Renewables and Efficiency	
	Spot market	Reduced Need for Balancing Power	PR	SR NEG	SR POS	TR NEG	TR POS	Reduced Grid Fees	PV self-consumption	Efficiency
Technical	Timescales suitable for HP	Suitable for HP, though frequent switching has to be avoided	Danger of frequent switching if not taken care of by pool management	Suitable for HP, though frequent switching has to be avoided		Suitable for HP, though frequent switching has to be avoided, long calls might be problematic		HP suitable already today	Suitable for HP, frequent cycling needs to be avoided	Suitable for HP
Costs	Communication technology, pool management, market participation fees, efficiency losses	Communication technology, pool management, efficiency losses	Communication technology, pool management, market participation fees, prequalification, efficiency losses					Communication and controls	Energy management, efficiency losses	Communication and energy management, efficiency losses
Revenue	low	medium	medium	medium	medium	low	low	high	medium	medium
Risk &	low	medium	high	high	high	high	high	low	low	low
Complexity										
Attractiveness	medium	medium	low	medium		low		high	high	high

good
moderate
poor

It has been shown that under current market conditions there is little incentive in terms of additional revenue for using HP in the different markets or on the level of a balance unit, compared to already existing business models (BM) that merely focus on improving local conditions or exploiting grid regulations. The alternatives that will lead to a full "smart" integration of heat pumps into a future energy system are more complex and risky, but offer additional revenue potentail. The estimated revenue of these different business models varies considerably from approximately 10€/$kW_{HP,el}$/year in case of BM1 to 120€/$kW_{HP,el}$/year with BM6. BM2 and BM8 offer the second highest revenue potential after BM6, with around 60€/$kW_{HP,el}$/year.
Besides the revenue potential, costs, technical requirements and possible risks should be considered as well. First of all, participating in the markets require the pooling of heat pump units in order to achieve the minimum capacity. The contracted flexibility must be guaranteed at all times, taking into account the variations based on its influencing factors, while respecting the comfort requirements of the dwellers, otherwise risking the viability of the business model. Secondly, most of these business models rely on communication

technologies with different levels of reliability requirements, which adds costs and complexity. The business models targeting on efficiency increase of heat pumps are attractive and comparably simple to realise. Hence, these are expected to be established first. From a technical point of view of a single heat pump unit, the market for primary and secondary reserve is not very attractive as frequent changes in operation are required. The calculated revenue potential does not seem to justify the technical stress to the system. However, in a large pool frequent switching can be avoided at the cost of lower revenues. In this regard the tertiary reserve is the most favourable, but these models offer very low revenues due to the very low amount of time it is being called.

The analyses made by Fischer et at. highlights that technical aspects are crucial for a successful implementation of business models for flexibility. Communication devices, control and forecasting algorithms have to be further developed and should find their way from research into practice. Furthermore the influence of changed operating conditions should be studied in detail to quantify possible losses and a reduction in unit lifetime. System sizing, controls and system layout should be studied in detail to enable recommendations for a future heat pump system design that enables more flexibility [67].

Chapter 6

Conclusions

6.1 Conclusions

In this thesis, I have investigated the performance of data driven models of hot water systems, using deep neural networks. It can be concluded, that the used model architecture was able to capture the non-linear system dynamics and performed very well with given sufficient data was available. With incorporated domain knowledge, the model was able to perform well even outside the encountered state space. Increasing amount of data asymptotically increases the model performance, which is further accelerated in case of a multi-agent formulation due to the higher state space exploration. Storage vessel models required around 500 weeks of data to reach full performance, while the heat pump models take up to 1000 weeks due to the lower frequency of the observations. Even though the used methodology is fully generalizable, the models themselves perform best on a single type of equipment. In situations where the data is limited a model trained on a similar vessel could substitute temporarely with modest results.

The additional knowledge gained by these models makes it possible to use more sophisticated control strategies. As demonstrated, even a simple controller using the state of charge instead of a single temperature measurement can result in up to 65% of consumption reduction depending on the sensors location.

I have also analysed the different determinants of energy flexibility in hot water systems. While similar to the determinants of energy consumption in a building, there are nevertheless important differences. The most important of these is in the way occupant behaviour influences available flexibility.

Ambient conditions, including diurnal and seasonal variations in temperature, play a major role in determining the extent to which a hot water system can be operated flexibly to provide value added services. In general, device flexibility is highest during (cold) winter nights and lowest during (warm) summer afternoons.

The choice of control algorithm plays a rather surprisingly large role in the available flexibility. With the energy efficient controller, I show that it is also possible to elicit higher capacity on average from the same hot water system, albeit increasing the recovery period. This suggests at least one additional way for optimal control where controllers can be designed based on grid requirements.

Finally, occupant behaviour also influences device flexibility, though not as much as it influences actual energy consumption. There are numerous reasons for this. Primarily, available flexibility is limited by constraints on occupant comfort which ensure that the system can only be operated within certain bounds. Furthermore, occupant behaviour works in tandem with thermodynamic losses to determine the capacity and recovery period of a device. This means that increasing hot water demand for users leads to only

somewhat higher capacity, similar to the use of a more efficient controller. However, unlike with the controller, higher consumption also leads to a generally shorter recovery period. This means that households with higher consumption can provide more flexibility to the grid, more often. This difference can be rather substantial with recovery periods varying by a factor of almost three.

While we have used a heat pump hot water system in our analysis, the presented framework is completely generalizable. There remain however important qualifications for the generalizability of the results. Foremost among these is the disproportionate effect ambient conditions has on device flexibility. In many instances, these can single-handedly alter a system?s available capacity by a factor of more than two. This result therefore only holds for a heat pump system in a strict sense because of its temperature dependent efficiency. In a system employing a different heating element, such as an electric resistance heater or gas boiler, this effect would still persist but in a much diminished form.

The fact that different controllers and occupant behaviour influence energy flexibility significantly further complicates its quantification in a standard form by adding yet another degree of freedom. This information must be utilized in future research on quantification of device flexibility.

This analysis of the flexibility of hot water systems has important repercussions for the use of hot water systems in grid supportive roles. More concretely, in most Northern European countries, hot water systems have been considered as a means to reduce the peak injection of solar production during the summer months. However, the flexibility of such devices is generally at its lowest during this period. This information, and not the average flexibility of these devices, has to be taken into consideration during operational planning of modern grids. In the more general context, care must be taken to account for these differences in energy flexibility of the same system which can vary by as much as three to four times depending on ambient conditions, occupant behaviour and choice of controller.

Bibliography

[1] Intergovernmental Panel on Climate Change and T. Stocker. *Climate Change 2013: The Physical Science Basis: Working Group I Contribution to the Fifth Assessment Report of the Intergovernmental Panel on Climate Change*. Cambridge University Press, 2014. URL: https://books.google.be/books?id=o4gaBQAAQBAJ.

[2] United Nations. "Paris Agreement". In: (2015).

[3] *Energy Efficiency Directive - Directive 2012/27/EU*. URL: https://eur-lex.europa.eu/legal-content/en/TXT/?uri=celex:32012L0027.

[4] *The 2020 climate & energy package*. URL: https://ec.europa.eu/clima/policies/strategies/2020_en (visited on 05/07/2018).

[5] *The 2030 climate & energy framework*. URL: https://ec.europa.eu/clima/policies/strategies/2030_en (visited on 05/07/2018).

[6] European Comission. "Proposal for a Directive of the European Parliament and of the Council amending Directive 2010/31/EU on the energy performance of buildings". In: (2016).

[7] *Energy Performance of Buildings - Directive 2010/31/EU*. URL: https://eur-lex.europa.eu/legal-content/EN/TXT/?uri=COM:2016:765:FIN (visited on 07/05/2018).

[8] Magnus Bonde and Han Suck Song. "Does Greater Energy Performance have an Impact on Real Estate Revenues?" In: *Journal of Sustainable Real Estate* 5.1 (2014), pp. 171–182. URL: http://aresjournals.org/doi/abs/10.5555/jsre.5.1.q8r85u3112r15g22.

[9] Piotr Kowalski and Szala´nski Pawel. "Computational and the real energy performance of a single-family residential building in Poland - an attempt to compare: a case study". In: *E3S Web Conf.* 17 (2017). URL: https://doi.org/10.1051/e3sconf/20171700045.

[10] D. Majcen, L.C.M. Itard, and H. Visscher. "Theoretical vs. actual energy consumption of labelled dwellings in the Netherlands: Discrepancies and policy implications". In: *Energy Policy* 54.C (2013), pp. 125–136. URL: https://EconPapers.repec.org/RePEc:eee:enepol:v:54:y:2013:i:c:p:125-136.

[11] Pantelis Capros et al. "European decarbonisation pathways under alternative technological and policy choices: A multi-model analysis". In: *Energy Strategy Reviews* 2.3 (2014), pp. 231–245. URL: http://www.sciencedirect.com/science/article/pii/S2211467X13001053.

[12] Agora Energiewende. "The Integration Cost of Wind and Solar Power. An Overview of the Debate on the Effects of Adding Wind and Solar Photovoltaic into Power Systems". In: *Agora Energiewende: Berlin, Germany* (2015).

[13] M. De Grote, V. Volt, and O. Rapf. *Smart Buildings in a Decarbonised Energy System Building*. 2016.

[14] Søren Østergaard Jensen. "IEA EBC Annex 67 Energy Flexible Buildings". In: (2016). URL: http://www.annex67.org/media/1057/ebc_annex_67_annex_text.pdf.

[15] Adam Nagy et al. "Deep Reinforcement Learning for Optimal Control of Space Heating". In: (2018).

[16] Thomas Mertens. "Evaluating the use of distributed and centralized black box models to predict DHW characteristics". MA thesis. KU Leuven, 2017.

[17] Hussain Kazmi, Johan Suykens, and Johan Driesen. "Multi-agent Reinforcement Learning for Modelling and Control of Thermostatically Controlled Loads". 2018.

[18] M. K. Petersen et al. "A taxonomy for modeling flexibility and a computationally efficient algorithm for dispatch in Smart Grid". In: *American Control Conference* (2013).

[19] Daan Six et al. "Exploring the flexibility potential of residential heat pumps combined with thermal energy storage for smart grids". In: *21st International conference on electricity distribution* 0442 (2011).

[20] W. Cardinaels and I. Borremans. *Demand response for families – linear final report*. 2014. URL: http://www.linear-smartgrid.be/sites/default/files/Linear%20Final%20Report%20-%20lr2.pdf.

[21] Frauke Oldewurtel et al. "Towards a Standardized Building Assessment for Demand Response". In: *51nd IEEE conference on Decision and Control* (2013).

[22] Seung Ho Hong, Mengmeng Yu, and Xuefei Huang. "A real-time demand response algorithm for heterogeneous devices in buildings and homes". In: *Energy* 80.C (2015), pp. 123–132.

[23] Peter D. Lund et al. "Review of energy system flexibility measures to enable high levels of variable renewable electricity". In: *Renewable and Sustainable Energy Reviews* 45.P (2015), pp. 785–807.

[24] K.O. Aduda et al. "Demand side flexibility: potentials and building performance implications". In: *Sustainable Cities and Society* 22 (2016), pp. 146–163.

[25] C. Eid et al. "Aggregation of demand side flexibility in a smart grid: A review for European market design". In: *12th International Conference on the European Energy Market (EEM)* (2015), pp. 1–5.

[26] IEA EBC Annex 67: Energy Flexible Buildings. "Energy flexibility as a key asset in a smart building future contribution of annex 67 to the european smart building initiatives". In: *Annex 67 Position Paper* (Nov. 2017). URL: http://www.annex67.org/media/1470/position-paper-energy-flexibility-as-a-key-asset-i-a-smart-building-future.pdf.

[27] Niamh O'Connell et al. "Benefits and challenges of electrical demand response: A critical review". In: *Renewable & Sustainable Energy Reviews* 39 (2014), pp. 686–699.

[28] Usman Ijaz Dar et al. "Advanced control of heat pumps for improved flexibility of Net-ZEB towards the grid". In: *Energy & Buildings* 69 (2014).

[29] Jérôme Le Dréau and Per Heiselberg. "Energy flexibility of residential buildings using short term heat storage in the thermal mass". In: *Energy* 111 (Sept. 2016), pp. 991–1002.

[30] G. Reynders, J. Diriken, and D. Saelens. "A generis quantification method for the active demand response potential of structural storage in buildings". In: *14th Conference of International Building Performance Simulation Association* (2015). URL: http://www.ibpsa.org/proceedings/BS2015/p2475.pdf.

[31] Sebastian Stinner, Kristian Huchtemann, and Dirk Müller. "Quantifying the operational flexibility of building energy systems withthermal energy storages". In: *Applied Energy* 181 (2016), pp. 140–154.

[32] Th Nuytten et al. "Flexibility of a combined heat and power system with thermal energy storage for district heating". In: *Applied Energy* 104 (2013), pp. 583–591.

[33] Jyri Salpakari and Peter Lund. "Optimal and rule-based control strategies for energy flexibility in buildings with PV". In: *Applied Energy* 161 (2016), pp. 425–436. URL: http://urn.fi/URN:NBN:fi:aalto-201705114163.

[34] Samuel Prıvara et al. "Building modeling as a crucial part for building predictive control". In: *Energy and Buildings* 56 (2012), pp. 8–22.

[35] J. Cigler and S. Prıvara. "Subspace identification and model predictive control for buildings". In: *11th International Conference on Control Automation Robotics Vision* (2010), pp. 750–755.

[36] Lukáš Ferkl and Jan Široký. "Ceiling radiant cooling: Comparison of ARMAX and subspace identification modelling methods". In: *Building and environment* 45.1 (2010), pp. 205–212.

[37] A.E. Ruano et al. "Prediction of building's temperature using neural networks models". In: *Energy and Buildings* 38 (2006), pp. 682–694.

[38] S. Wang and X. Xu. "Simplified building model for transient thermal performance estimation using GA-based parameter identification". In: *International journal of thermal sciences* 45.4 (2006), pp. 419–432. URL: http://hdl.handle.net/10397/15853.

[39] Anita Martincevic, Mario Vašak, and Vinko Lešic. "Model Predictive Control for Energy-saving and Comfortable Temperature Control in Buildings". In: ().

[40] Jan Široký et al. "Experimental analysis of model predictive control for an energy efficient building heating system". In: *Applied Energy* 88.9 (2011), pp. 3079–3087.

[41] Peder Bacher and Henrik Madsen. "Identifying suitable models for the heat dynamics of buildings". In: *Energy and Buildings* 43.7 (2011), pp. 1511–1522.

[42] D. Subbaram Naidu and Craig G. Rieger. "Advanced control strategies for heating, ventilation, air-conditioning, and refrigeration systems — An overview: Part I: Hard control". In: *HVAC&R Research* 17.1 (2011), pp. 2–21. URL: https://www.tandfonline.com/doi/abs/10.1080/10789669.2011.540942.

[43] Abdul Afram and Farrokh Janabi-Sharifi. "Theory and applications of HVAC control systems – A review of model predictive control (MPC)". In: 72 (Feb. 2014), pp. 343–355.

[44] A.I. Dounis and C. Caraiscos. "Advanced Control Systems Engineering for Energy and Comfort Management in a Building Environment—A Review." In: *Renewable and Sustainable Energy Reviews Journal* 13 (2009), pp. 1246–1261.

[45] D. J. Leith and W. E. Leithead. "Survey of gain-scheduling analysis and design". In: *International Journal of Control* 73.11 (2000), pp. 1001–1025. URL: https://doi.org/10.1080/002071700411304.

[46] Matthew Lai. "Giraffe: Using Deep Reinforcement Learning to Play Chess". In: *CoRR* abs/1509.01549 (2015). URL: http://arxiv.org/abs/1509.01549.

[47] Volodymyr Mnih et al. "Human-level control through deep reinforcement learning". In: *Nature* 518 (2015). URL: http://dx.doi.org/10.1038/nature14236.

[48] David Silver et al. "Mastering the game of Go with deep neural networks and tree search". In: *Nature* 529 (2016). URL: http://dx.doi.org/10.1038/nature16961.

[49] Simeng Liu and Gregor P. Henze. "Experimental analysis of simulated reinforcement learning control for active and passive building thermal storage inventory Part 1. Theoretical foundation". In: *Energy and Buildings* 38 (2006), pp. 142–147.

[50] E. Barrett and S. Linder. "Autonomous hvac control, a reinforcement learning approach', in Lecture Notes in Computer Science (including subseries Lecture Notes in Artificial Intelligence and Lecture Notes in Bioinformatics)". In: (2015), pp. 3–19.

[51] Lei Yang et al. "Reinforcement learning for optimal control of low exergy buildings". In: *Applied Energy* 156.C (2015), pp. 577–586.

[52] A. Ali and H. Kazmi. "Minimizing Grid Interaction of Solar Generation and DHW Loads in nZEBs Using Model-Free Reinforcement Learning." In: *In: Woon W., Aung Z., Kramer O., Madnick S. (eds) Data Analytics for Renewable Energy Integration: Informing the Generation and Distribution of Renewable Energy. DARE 2017. Lecture Notes in Computer Science* 10691 (2017).

[53] Tianshu Wei, Yanzhi Wang, and Qi Zhu. "Deep Reinforcement Learning for Building HVAC Control". In: *Proceedings of the 54th Annual Design Automation Conference* (2017).

[54] Christian Finck et al. *Review of applied and tested control possibilities for energy flexibility in buildings - A technical report from IEA EBC Annex 67 Energy Flexible Buildings*. May 2018.

[55] David H. Wolpert. "The Supervised Learning No-Free-Lunch Theorems". In: *Soft Computing and Industry: Recent Applications*. Ed. by Rajkumar Roy et al. Springer London, 2002, pp. 25–42. URL: https://doi.org/10.1007/978-1-4471-0123-9_3.

[56] Kevin P. Murphy. *Machine Learning A Probabilistic Perspective*. The MIT Press, 2012.

[57] Simon Haykin. *Neural Networks*. Pearson Education, 1999.

[58] Q. J. Zhang. *Neural Networks for RF and Microwave Design*. Artech House, 2000.

[59] *Stanford CS231*. URL: http://cs231n.github.io/neural-networks-1/ (visited on 05/07/2018).

[60] *Enervalis*. URL: https://www.enervalis.com (visited on 05/07/2018).

[61] Y.M. Han, R.Z. Wang, and Y.J. Dai. "Thermal stratification within the water tank". In: *Renewable and Sustainable Energy Reviews* 13.5 (2009), pp. 1014–1026. URL: http://www.sciencedirect.com/science/article/pii/S1364032108000385.

[62] *Keras documentation*. URL: https://keras.io (visited on 05/07/2018).

[63] *Python Software Foundation*. URL: https://www.python.org (visited on 05/07/2018).

[64] Kaiming He et al. "Delving Deep into Rectifiers: Surpassing Human-Level Performance on ImageNet Classification". In: *CoRR* abs/1502.01852 (2015). URL: http://arxiv.org/abs/1502.01852.

[65] Günter Klambauer et al. "Self-Normalizing Neural Networks". In: *CoRR* abs/1706.02515 (2017). URL: http://arxiv.org/abs/1706.02515.

[66] Diederik P. Kingma and Jimmy Lei Ba. "ADAM: A method for stohastic optimization". In: *ICLR* (2015).

[67] David Fischera et al. "Business Models Using the Flexibility of Heat Pumps – A Discourse". In: *12th IEA Heat Pump Conference* (2017).